

A DUAL RANDOM DOMAIN LIBRARY STRATEGY FOR APTAMER SELECTIONS: TARGETING SARS-COV-2 SPIKE PROTEIN AS A MODEL FOR PANDEMIC PREVENTION

BY

RYAN AMINI

B.Sc. McMaster University, Hamilton, Ontario, 2022

A Thesis Submitted to the School of Graduate Studies in Partial Fulfillment of the Requirements for the Degree Master of Science

McMaster University © Copyright by Ryan Amini, July 2024

MASTER OF SCIENCE (2024)
Biochemistry & Biomedical Sciences
McMaster University
Hamilton, Ontario
TITLE:
A Dual Random Domain Library Strategy for Aptamer Selections
AUTHOR:
Ryan Amini, B.Sc. (McMaster University)
SUPERVISOR:
Professor Dr. Yingfu Li
NUMBER OF PAGES: 61

ABSTRACT

Multimeric aptamer strategies are often adopted to improve the binding affinity of an aptamer toward its target molecules. In most cases, multimeric aptamers are constructed by connecting pre-identified monomeric aptamers derived from in vitro selection. Although multimerization provides an added benefit of enhanced binding avidity, the characterization of different aptamer pairings adds more steps to an already lengthy procedure. Therefore, an aptamer strategy that directly selects for multimeric aptamers is highly desirable. Here, we report on an *in vitro* selection strategy using a pre-structured DNA library that forms dimeric aptamers. Rather than using a library containing a single random region, which is nearly ubiquitous in existing aptamer selections, our library contains two random regions separated by a flexible poly-thymidine (poly-T) linker. Following sixteen rounds of selection against the SARS-CoV-2 spike protein, a relevant model target protein due to the COVID-19 pandemic, the top aptamers found with our library displayed K_d values as low as 0.15 nM, which is consistent with other reported dimeric aptamers. As confirmed via dot blot analysis, each random region functions as a distinct binding moiety, but the regions work together to recognize the spike protein. Our library strategy provides an accelerated method to obtain high-binding dimeric aptamers, which may prove useful in future aptamer diagnostic and therapeutic applications.

ACKNOWLEDGEMENTS

I would like to express my gratitude to Dr. Yingfu Li, who first accepted me into the lab when I was a second-year undergraduate student. His trust in my abilities and continued support have been instrumental in my development as a researcher. I am also grateful to my committee members Dr. Leyla Soleymani and Dr. Hong Han for their time, effort, and constructive comments which significantly improved the quality of this thesis.

Additionally, I would also like to thank the many members of the Li Lab for contributing to such an enriching experience. Special thanks to my mentors, Dr. Zijie Zhang, Dr. Jiuxing Li, and Dr. Qing Wang, for providing me with incredible guidance. I would also like to give a shout-out to my best mates in the lab, Jake, Connor, and Amal, who have made my time in the lab so enjoyable.

Moreover, I gratefully acknowledge the financial support provided by the Natural Science and Engineering Research Council of Canada (NSERC), Canadian Institutes of Health Research (CIHR), Mitacs, and Zentek, which made this research possible.

Finally, I would like to thank my family. Their belief in me has been a source of strength throughout my academic journey. I would like to express my deepest appreciation to my parents and my brother, Parshawn, for their unwavering support.

I would like to dedicate this thesis to my family and friends, who have loved and supported me unconditionally. Your encouragement and belief in me have been invaluable.

TABLE OF CONTENTS

CHA	PTER 1: INTRODUCTION	1
1.1	Discovery of functional nucleic acids	1
1.2	Overview of nucleic acid aptamers	2
1.3	Binding affinity and aptamer multimerization	5
1.4	Dual random domain selection	7
1.5	COVID-10, SARS-CoV-2, and future pandemic prevention	10
1.6	Bead-based SELEX	11
1.7	Thesis objectives	14
СНА	PTER 2: MATERIALS AND METHODS	15
2.1	Chemicals and reagents	15
2.2	Overview of dual random domain SELEX protocol	15
2.3	Characterization of dual random domain aptamer binding	18
СНА	PTER 3: DRD APTAMER SELECTION AGAINST SARS-COV-2 S	22
PRO'	ΓΕΙΝ	22
3.1	Rationale of dual random domain library design	22
3.2	Deep sequencing of DNA pools	23
СНА	PTER 4: DRD APTAMER CHARACTERIZATION	25
4.1	Assessment of binding affinity of top 5 aptamer clusters for BA.5 S	25
protei	n	23
4.2	Binding of a pseudotyped Omicron BA.5 SARS-CoV-2 lentivirus by	27
DRD.	A-8 and DRDA-10	21
4.3	Multivalent characterization of DRDA-8 and DRDA-10	29

4.4	T-linker shortening analysis	36
4.5	Selectivity assessment of DRDA-8 and DRDA-10	38
CHAPTER 5: CONCLUSION AND FUTURE DIRECTIONS		40
SUPPORTING INFORMATION		42
REFE	ERENCES	58

LIST OF FIGURES AND TABLES

Figure 1.1. Illustration of SELEX procedure	4
Figure 1.2. Overview of dual random domain selection approach	9
Figure 1.3. Schematic outline of magnetic bead-based SELEX protocol	13
Figure 2.1. Illustration of electromobility shift assay (EMSA) and dot blot assay	20
for characterization of aptamer binding	20
Figure 4.1. DRD aptamer library and the resulting high-affinity DRD aptamers	26
Figure 4.2. Assessment of binding affinity of DRDA-8 and DRDA-10 to	
pseudotyped lentiviruses (PV) engineered to display the Omicron BA.5 S protein	28
of SARS-CoV-2	
Figure 4.3. Truncation analysis of DRDA-8 and DRDA-10	31
Figure 4.4. Competition between DRDA-8 Truncation 1 and DRDA-8 Truncation	34
2 for binding to the S protein	34
Figure 4.5. Competition between DRDA-8 Truncation 2 and DRDA-8 Truncation	35
or binding to the S protein	
Figure 4.6. DRD aptamer poly-T linker analysis	37
Figure 4.7. Selectivity assessment of DRDA-8 and DRDA-10	39
Table S1. All synthetic oligonucleotides utilized in this study	42
Table S2. Concentrations of DNA and protein used during SELEX	44
Table S3. Top 50 ranking sequences in pool 16 ranked by their percentage	45
Table S4. Top 50 ranking sequences in pool 16 organized by their class	47
Table S5. Sequence classes of left domain observed in Top 50 sequences	49
Table S6. Sequence classes of right domain observed in Top 50 sequences	50

Table S7. K _d values of reported aptamers for the SARS-CoV-2 spike protein	51
Figure S1. Assessment of binding of selected enriched pools for Omicron BA.5 S	52
protein target	32
Figure S2. Assessment of binding affinity of top DRD aptamers for the Omicron	53
BA.5 S protein	33
Figure S3. The predicted secondary structure of DRDA-8 and the binding affinity	54
of its truncated mutants	
Figure S4. The predicted secondary structure of DRDA-10 and the binding affinity of its truncated mutants	
sequences	30
Figure S6. MUSCLE alignment comparison of DRD aptamers to a selection of	57
published SARS-CoV-2 spike aptamer sequences	51

LIST OF ABBREVIATIONS AND SYMBOLS

ATP adenosine 5'-triphosphate

COVID-19 coronavirus disease 2019

ddH2O double distilled water, nuclease free

DNA deoxyribonucleic acid

DNAzyme DNA enzyme

dNTP 2'-deoxynucleoside 5'-triphosphate

dPAGE denaturing polyacrylamide gel electrophoresis

DRD dual random domain

DRDA DRD aptamer

EDTA ethylenediaminetetraacetic acid

EMSA electrophoretic mobility shift assay

FNA Functional nucleic acid

*K*_d dissociation constant

MUSCLE Multiple Sequence Comparison by Log-Expectation

nt nucleotide

PCR polymerase chain reaction

PNK polynucleotide kinase

Poly-T poly-thymidine

RAT rapid antigen test

RNA ribonucleic acid

SARS-CoV-2 severe acute respiratory syndrome coronavirus 2

SB selection buffer

SELEX Systematic Evolution of Ligands by Exponential Enrichment

ssDNA single stranded DNA

CHAPTER 1: INTRODUCTION

1.1 Discovery of functional nucleic acids

For many years, nucleic acids were strictly regarded as carriers of genetic information. DNA was viewed only as the genetic blueprint, with RNA acting as an intermediary in protein synthesis. However, over the late twentieth century, this perspective changed. Apart from their role as hereditary material in living systems, nucleic acids have more recently been discovered to function as regulators, enzymes, and ligands.^[1]

The initial breakthroughs came with the discovery of ribozymes in the early 1980s, which demonstrated that RNA molecules could possess catalytic functions, including the cleavage and ligation of phosphodiester and peptide bonds. [2] Kruger *et al.*, for example, first revealed that precursor ribosomal RNA (rRNA) could self-splice in the absence of enzymes. [3] Additional studies then revealed that these catalytic activities were highly dependent on the three-dimensional structures that RNA molecules could adopt. [4,5] For instance, the hammerhead ribozyme, one of the most well-known ribozymes in nature, was discovered to fold into a specific three-dimensional shape that brings the catalytic core into the proper alignment to facilitate the cleavage of RNA. [6] These discoveries emphasized that nucleic acids could adopt specific structures to carry out functional roles beyond their canonical functions of genetic storage and transfer.

Inspired by these natural phenomena, researchers sought to develop synthetic nucleic acids with novel functionalities. By 1990, several groups had independently explored the idea of *in vitro* selection, a method for evolving functional nucleic acids (FNAs) with specific binding properties from a large pool of random sequences. Tuerk and Gold isolated RNA sequences that bound to T4 DNA polymerase, while Ellington and Szostak found RNA molecules that

specifically bound to organic dyes.^[7,8] These discoveries underscored the vast potential of nucleic acids as versatile ligands for various targets, both organic and inorganic. These nucleic acid molecules were named aptamers, and since then, they have been widely studied in diagnostics, therapeutics, and biotechnology.

1.2 Overview of nucleic acid aptamers

Aptamers are single-stranded nucleic acid ligands that fold into well-defined structures capable of binding to a target of interest. [9,10] Their binding capability is akin to that of antibodies, earning aptamers the name "chemical antibodies". [11] The term "aptamer" itself is derived from the Latin word "aptus," meaning "to fit," and the Greek word "meros," meaning "part," reflecting their ability to precisely fit and bind to target molecules. [8] Aptamers are able to bind to their targets by forming specific three-dimensional shapes through intramolecular interactions, such as hydrogen bonding, base stacking, and electrostatic forces. [12] This structural adaptability allows them to recognize and bind to a wide variety of molecules, including proteins, small molecules, ions, and even cells. [13] The binding interaction between an aptamer and its target is highly specific and often characterized by high affinity. For this reason, aptamers have become of great interest in the field of molecular detection. They are currently being studied as molecular recognition elements (MREs) for biosensing, diagnostics, therapeutics, molecular imaging, drug delivery, and gene therapy. [14]

Nucleic acid aptamers are derived using a process known as *in vitro* selection or SELEX (Systematic Evolution of Ligands through Exponential Enrichment) (**Figure 1.1**).^[7,8] The SELEX procedure begins with the synthesis of a library of 10¹⁵ single-stranded DNA or RNA sequences. Each sequence of the library is composed of a region of completely randomized nucleotides that are flanked by two primer-binding domains. In theory, each library will contain

several sequences that favourably interact with the target of interest. To generate functionally active sequences, the single-stranded library is incubated with the target to promote binding. Afterward, both the target and unbound sequences are discarded, while bound sequences are amplified via PCR. Finally, following successful amplification, the single-stranded nucleotide sequences in the pool are regenerated from the double-stranded PCR product. The retained sequences are used as the library in the following rounds, and the process is then repeated several times to enrich aptamers with the highest affinity and specificity. Once the pool exhibits satisfactory binding qualities, the DNA or RNA in the final round is sequenced to reveal the top-performing aptamers.^[15]

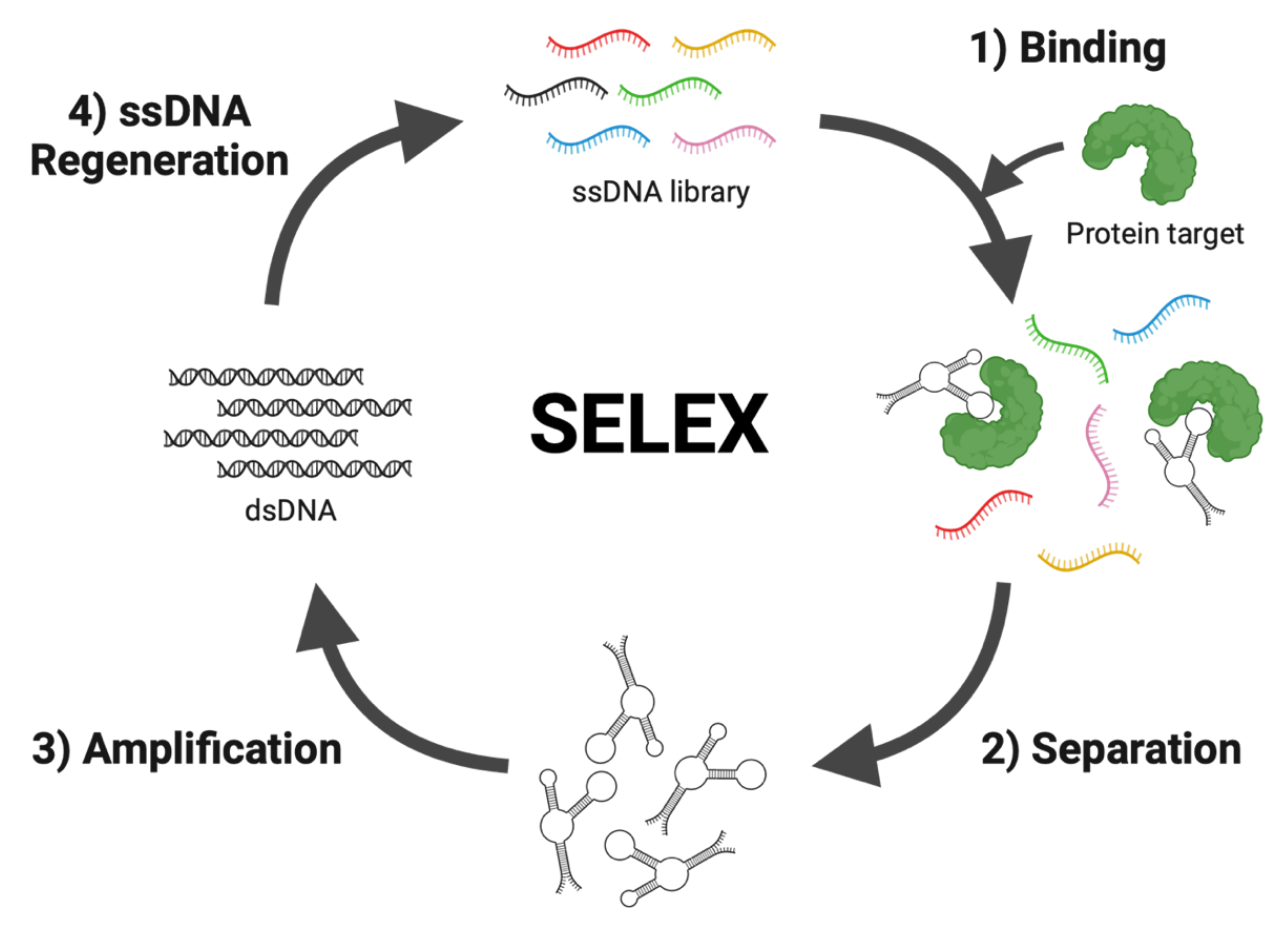


Figure 1.1. **Illustration of SELEX procedure**. SELEX (systematic evolution of ligands by exponential enrichment) begins with a large, random ssDNA library. A target, such as a protein, is incubated with the library to allow binding to occur. Bound sequences are then separated from the discarded unbound sequences and amplified via PCR. Once the library is regenerated, the enriched pool is used for a new round of selection until the aptamers exhibit satisfactory binding to the target.

Aptamers embrace a variety of advantages. As previously mentioned, aptamers can bind to targets with high affinity and high specificity (i.e., they bind tightly to their intended target and only to their intended target). Compared to antibodies as MREs, aptamers possess many advantages. Firstly, aptamers are both chemically and thermally stable, providing a relatively long shelf life. Secondly, since aptamers are synthesized *in vitro*, their production can be scaled with minimal batch-to-batch variation, and they avoid any exploitation of biological systems. Thirdly, each component of a nucleic acid (i.e., nucleotide base, sugar ring, and phosphate group) can be easily modified to fit the needs of an aptamer's intended purpose. Finally, in comparison to antibodies, aptamers are highly cost-effective. Given their desirable qualities, aptamers have been intensively investigated in FNA research, and their impact and applications will only continue to grow.

1.3 Binding affinity and aptamer multimerization

An important characteristic of aptamers is the strength of the binding interaction between the nucleic acids and the target, otherwise known as the binding affinity. This is typically measured using the dissociation constant (K_d), which quantifies the equilibrium between the bound and unbound states of the aptamer-target complex.^[22] The K_d value represents the concentration of the target at which half of the aptamer molecules are bound to the target, providing a precise metric for assessing the binding strength. Lower K_d values indicate higher affinity, signifying a more stable and tighter interaction between the aptamer and its target molecule.

Most aptamers in literature possess a respectable nanomolar level of binding affinity, which is akin to similar biomolecules such as antibodies.^[23,24] However, it can be difficult to push beyond this level of affinity for a number of reasons. Firstly, most SELEX experiments produce monomeric-binding aptamers that only bind to one epitope or subunit on the target. Secondly,

most selections are performed, on average, with 40 nucleotides in the random region. This is typically done to preserve the sequence space (i.e., the total number of possible sequences that can be generated for a given number of nucleotides). However, the use of these shorter random regions prevents the generation of more complex secondary structures, further limiting the interaction interface between the aptamer and the target.^[25]

To mitigate this issue and increase binding affinity, many aptamer groups use a multivalent strategy post-selection. Multivalent interactions occur when a single biomolecule simultaneously forms several binding interactions with its respective target. [26] This phenomenon is commonly observed in biology when precise molecular recognition is needed (e.g., when antibodies bind tightly to multiple sites on their respective antigens using their Y-shape scaffold). [27,28] With more than one ligand-binding site, the binding site's local concentration increases, as does the probability of an interaction. [29] In addition to increasing the rate of association, multivalency also reduces the rate of dissociation. If one binding site temporarily dissociates, the other sites remain bound, maintaining the overall complex and facilitating quick rebinding of the dissociated site. This results in a more stable and tighter interaction compared to monovalent binding. Therefore, not surprisingly, the strategy of multivalency and multimerization has been applied to aptamer ligands. [30-33]

Our group in the Yingfu Li Lab, for example, has had recent success in engineering both dimeric and trimeric aptamers for the SARS-CoV-2 spike protein that demonstrated exceptional improvement in affinity when compared to the monomeric aptamer substituent.^[34–36] Yet, this approach to constructing multimeric and multivalent aptamers can be a tedious trial-and-error process. It often necessitates finding two aptamers from a diverse pool that (1) bind to different

sites or subunits on the same target and (2) work well in tandem.^[33] Additionally, the process of characterizing multimeric aptamers adds more time to an already lengthy selection procedure.

It comes as no surprise that several aptamer groups have tried to solve this problem by directly selecting for multimeric aptamers. Adopting such a strategy would save several weeks in the process and eliminate the characterization steps of aptamer multimerization (i.e., analyzing sequences, characterizing top aptamers, and finding suitable aptamer pairs in a trial-and-error process). As an example, Zhou *et al.*, in 2019, fixed two separate random regions between a self-folding two-helix tile, achieving aptamers with a femtomolar affinity for thrombin.^[37] More recently, Tang *et al.* developed a DNA framework library that mimicked the Y-shaped scaffold of an antibody.^[38] Their resulting antibody-mimicking multivalent aptamers (Amap) showed great binding affinity and cooperativity to the protein target. Therefore, the idea of directly selecting for multivalent and multimeric aptamers is a valuable approach that could significantly streamline the development of high-affinity aptamers.

1.4 Dual random domain selection

Whilst the two listed studies of bivalent aptamer selections demonstrate innovative approaches in achieving high-affinity aptamers, each method comes with its own set of limitations. In the former example from Zhou $et\ al.$, an exceptionally low K_d value was achieved. However, the paranemic crossover method requires a complicated design, which may limit the streamlining for other targets. In the latter example from Tang $et\ al.$, the dissociation constant of the Amap aptamers did not exceed the nM range despite their intuitive antibody-mimicking approach.

Additionally, both of these selection strategies also used a rigid linker, which can be less adaptable to variations in the target shape. Flexible linkers, such as the poly-thymidine (poly-T)

linker, can be more advantageous for certain targets because they allow for greater freedom of movement and help the aptamer adapt to the three-dimensional shape of the target.^[32] To the best of our knowledge, no group in the functional nucleic acid literature has directly selected for multimeric aptamers using a flexible poly-nucleotide linker.

The Li Lab has taken a novel approach to directly select for multimeric aptamers. Termed the dual random domain (DRD) library, our library contains two 25-nucleotide random regions that are separated by a pre-structured 20-nucleotide poly-thymidine (poly-T) linker (**Figure 1.2**). Each 25-nucleotide random domain is hypothesized to form its own separate binding element by forming distinct secondary structures (i.e., hairpins, bulges, loops). However, with sufficient separation from the flexible poly-T linker, both random regions can potentially work synergistically and emulate the dual-arm binding effect seen in dimeric and bivalent aptamers. By implementing this strategy, we can possibly select for aptamers that have a higher affinity than those selected using a single random region, all while saving several months in the typical multivalent aptamer development process. Therefore, given these potential merits, the DRD selection method for aptamer development must be tested, challenged, and validated.

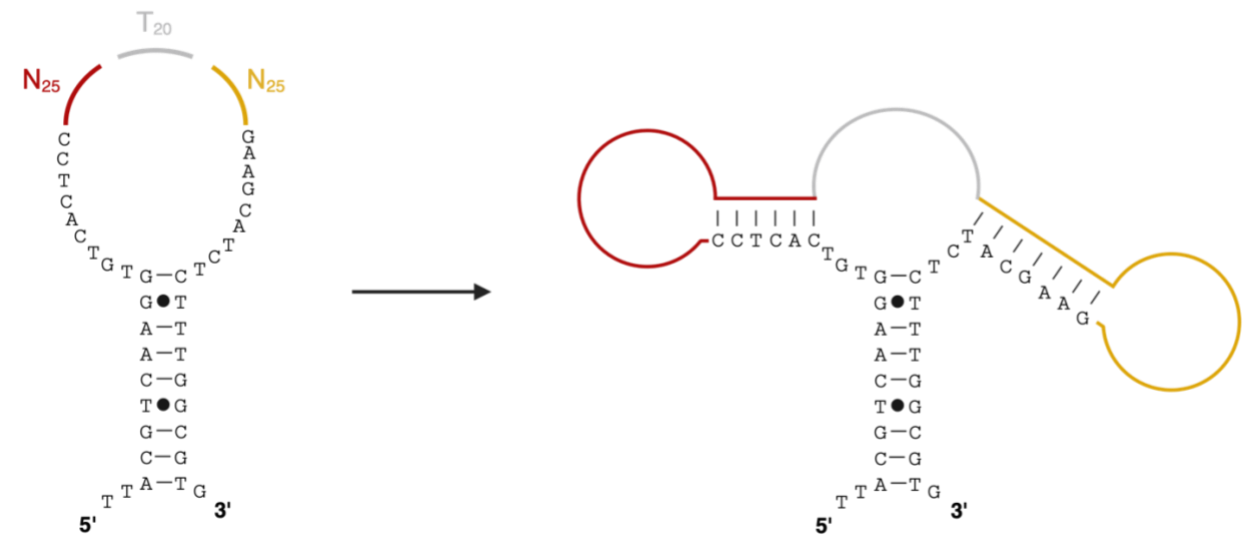


Figure 1.2. Overview of dual random domain selection approach. The dual random domain DNA library is pre-engineered with a primer set that forms a hairpin, two 25-nucleotide random regions, and one 20-nucleotide poly-T linker. By splitting the random region into two domains, and separating them with a flexible linker, the resultant aptamers from the selection are hypothesized to form dual-arm structures, similar to typical dimeric aptamers.

1.5 COVID-19, SARS-CoV-2, and future pandemic prevention

To test the validity of the DRD selection approach, the SARS-CoV-2 (severe acute respiratory syndrome coronavirus 2) spike (S) protein was chosen as the target. Although the threat of SARS-CoV-2 and the resulting COVID-19 disease (coronavirus disease 2019) have diminished over time, their widespread ramifications have left a lasting impression on the health and well-being of the global population. Since its initial outbreak in late 2019, a total of 650 million cases and 7 million deaths have been recorded. The pandemic impacted and continues to impact key aspects of a functioning society. Prolonged periods of quarantine took a toll on mental health, the massive influx of patients with COVID-19 led to major strains on healthcare infrastructure, and the world economy experienced its greatest recession in over a century. Fortunately, with the implementation of effective public health policies and the continuous administration of vaccines, COVID-19 will eventually reach an endemic state.

However, even without COVID-19, our society has grown more and more susceptible to infectious disease outbreaks. A combination of rapid technological, demographical, and climatic change has contributed to this movement. [44] To prevent a similar catastrophe to that of COVID-19, we need the most effective, efficient, and readily available technologies to diagnose these novel and re-emerging pathogens. Proper diagnostic testing can allow for contact tracing, large-scale testing, and isolation, all of which control the spread of an infectious pathogen. [45,46] It is, therefore, extremely vital that we build from the diagnostic inadequacies of the ongoing pandemic.

Throughout COVID-19, diagnostic screening primarily relied on reverse transcriptionquantitative polymerase chain reaction (RT-qPCR) as the gold-standard, with rapid antigen testing (RAT) as a convenient supplementary. While PCR methods are highly sensitive and specific,^[47] they are also time-consuming, expensive, and laborious.^[48,49] Additionally, the technique requires a completely sterile environment. Otherwise, false-positives may ensue from contamination.^[50] All these drawbacks prevent PCR-based tests from acting in a point-of-care setting. Fortunately, RATs cut down on cost, complexity, and "sample-to-answer" time, but they sacrifice sensitivity and are therefore prone to false-negative results.^[51,52] On the therapeutic front, most treatments were limited early on as they had to be intravenously administered in a clinical setting.^[53] Oral pills such as Paxlovid eventually became more widespread, but the availability and distribution of these treatments were often uneven, and their effectiveness varied based on the timing of administration and individual patient factors.^[54]

Taken altogether, there is a clear need for improvement in the space of viral diagnostics and therapeutics, and the recent SARS-CoV-2 virus provides an excellent model to research and prepare for the next pandemic. The S protein, in particular, is an ideal protein target because it is a large intermembrane protein, it is trimeric (made of three subunits), it is highly abundant on the surface of the virus, and does not require lysis for access. [55,56] Therefore, given its characteristics, the S protein will serve as a robust candidate for studying the DRD library method.

1.6 Bead-based SELEX

Many different SELEX methodologies are available to test the DRD library strategy. The most popular method in the literature is bead-based SELEX.^[25] In this method, targets are tagged with functional groups that firmly attach to solid bead supports.^[57,58] Sequences that bind form aptamer-target-bead complexes in solution, and unbound sequences are separated either by aggregating the beads via centrifugation or magnetism. Bound aptamers are then eluted from the target-bead complex and are amplified for the following round.^[59]

An example of a functional group and bead interaction is the His-Ni-NTA interaction. ^[60] In this method, nickel-nitrilotriacetic acid (Ni-NTA) magnetic beads are coated with nickel ions that specifically bind to histidine (His)-tagged proteins. His-tags, consisting of 6-8 histidine residues typically engineered onto proteins, chelate with the nickel ions through coordination bonds. This affinity allows His-tagged proteins to be selectively immobilized onto the Ni-NTA magnetic beads, forming stable complexes essential for bead-based SELEX.

Bead-based SELEX is favoured because of its overall simplicity and its applicability to a wide range of targets due to the abundance of available protein tags.^[25] For the SARS-CoV-2 S protein, the Li Lab has experienced great success in isolating high-affinity aptamers using a magnetic bead-based approach.^[34,61] Thus, an experimental method can be designed to validate the DRD library selection strategy (**Figure 1.3**).

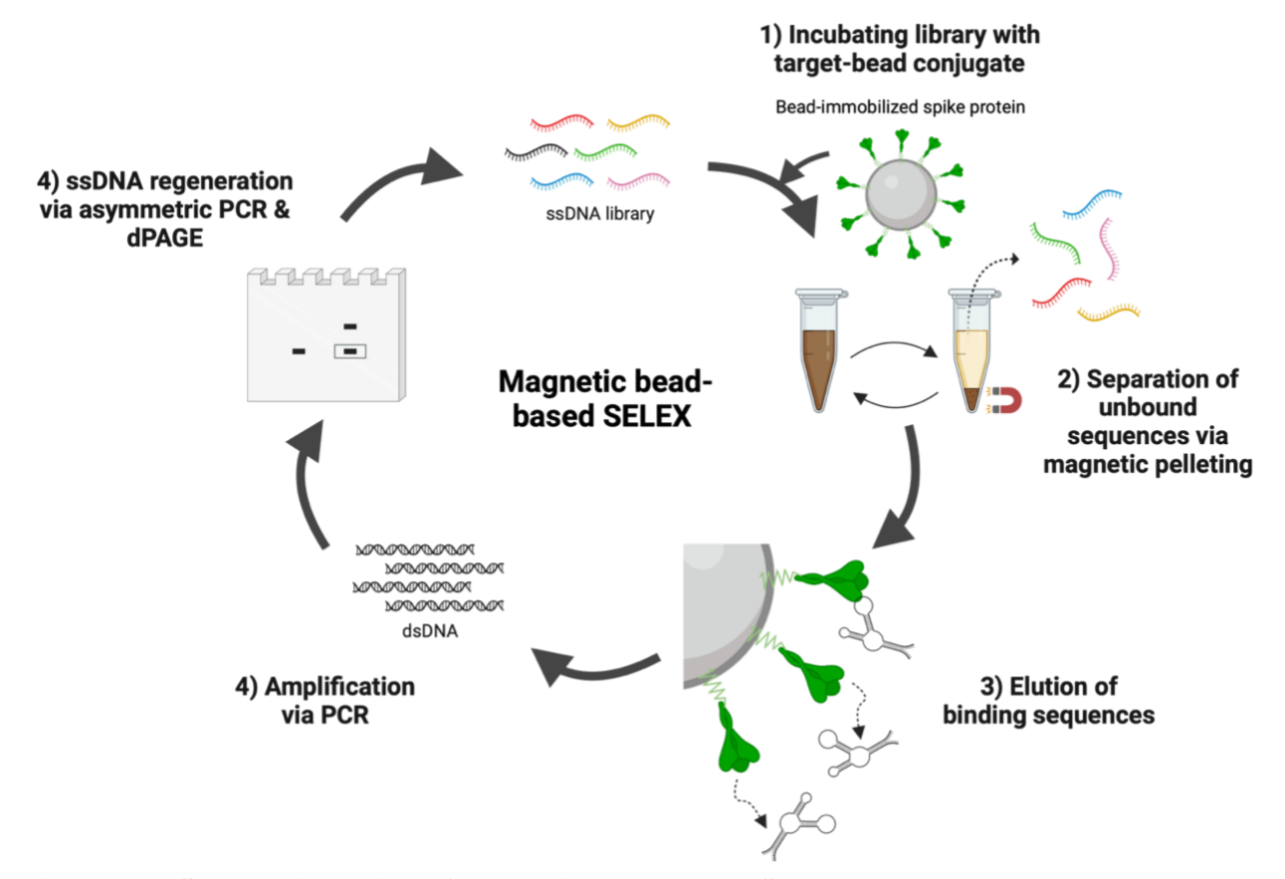


Figure 1.3. Schematic outline of magnetic bead-based SELEX protocol. The selection was completed using the DRD library (109 nt, 2 × 25N) with spike protein immobilized on magnetic Ni-NTA beads. (1) The DRD library and bead-immobilized spike protein were mixed and incubated on a shaker at RT for 2 hours. (2) Unbound sequences were removed by pelleting the magnetic bead and removing the supernatant via wash steps. (3) Binding sequences were eluted using a heat shock method, denaturing the non-covalent interactions between the aptamers and spike protein. (4) Eluted DNA was amplified using PCR 1 primers. (5) PCR 1 product was amplified using PCR 2 primers and the sense strand was separated from the antisense on a 10% dPAGE to regenerate ssDNA library. A total of 16 rounds were completed.

1.7 Thesis Objectives

The objective of this thesis is to assess the effectiveness of the DRD library selection strategy. It is hypothesized that the DRD selection library will provide higher-affinity aptamers in comparison to those selected using a single random region. To test this hypothesis, the S protein of the SARS-CoV-2 virus was chosen as the target. This protein also provides an excellent model and test case to simulate an aptamer development response to a future pandemic.

Therefore, the following experimental objectives were proposed for this thesis:

- Perform SELEX experiment with the DRD library and SARS-CoV-2 S protein, using a magnetic bead-based approach.
- Identify aptamer candidates from the selection and assess their binding properties for the S protein.
- 3) Examine 'dimeric-like' qualities of DRD aptamers and determine whether the DRD library strategy can be archived for future selection experiments that require a rapid generation of high-affinity dimeric aptamers.

CHAPTER 2: MATERIALS & METHODS

2.1. Chemicals and reagents

DNA oligonucleotides (DNA library, forward primer, reverse primer, reverse blocked primer) were purchased from Integrated DNA Technologies (IDT) and purified via standard 10% denaturing (8 M urea) polyacrylamide gel electrophoresis. The sequences of all the oligonucleotides used in this study are listed in **Table S1**. His-tagged SARS-CoV-2 spike trimer protein of the Omicron BA.5 subvariant (catalog number: SPN-C522e) were expressed from human embryonic kidney 293 cells (HEK293) and purchased from Acro Biosystems. HisPur Ni-NTA magnetic beads (catalog number: 88831) were purchased from Thermo Scientific. The SARS-CoV-2 spike-pseudotyped lentivirus for the Omicron BA.5 variant (Cat. No. 78652) was purchased from BPS Biosciences Inc. T4 polynucleotide kinase (PNK) and deoxyribonucleoside 5'-triphosphates (dNTPs) were purchased from Thermo Scientific (Ottawa, ON, Canada). [y-32P]-ATP was purchased from PerkinElmer. 96-well microtiter plates (clear, polystyrene, flat bottom) were from Celltreat Inc. Nitrocellulose membranes (Cat. No. 10600125) were from GE Healthcare Inc. Nylon membranes (Cat. No. NEF994001PK) were obtained from PerkinElmer Inc (Woodbridge, ON, Canada). Sodium chloride (NaCl), potassium chloride (KCl), HEPES (4-(2-hydroxyethyl)-1-piperazineethanesulfonic acid), sodium phosphate dibasic (Na₂HPO₄), potassium phosphate monobasic (KH₂PO₄), and Tween-20 were purchased from Sigma Aldrich. Milli-Q water was used for each experiment.

2.2. Overview of dual random domain SELEX protocol

Conjugation of SARS-CoV-2 spike trimer protein (BA.5/Omicron) on magnetic beads

HisPur Ni-NTA magnetic beads (5% w/v, 12.5 mg/mL) were utilized to immobilize the histidine-tagged SARS-CoV-2 Omicron BA.5 spike trimer protein (BA.5 S) of interest. 25 µL of beads was first aliquoted and washed with 500 µL of PBST buffer (500 µL, 137 mM NaCl, 2.7 mM KCl, 10 mM Na₂HPO₄, 1.8 mM KH₂PO₄, 0.01% v/v Tween-20). Afterward, 20.8 µL of Histagged BA.5 S and 54.2 µL of binding buffer (1× PBS, 0.01% v/v Tween-20) was added with the 25 µL magnetic beads and incubated at 4°C for 7 hours. The beads and protein were mixed to fulfill the maximum capacity of the magnetic beads. Given that the concentration of the beads was 12.5 μ g/ μ L and the capacity was 40 μ g of protein per mg of beads, the maximum amount of protein to be added for 25 µL of beads was 12.5 µg. Following the conjugation, the aqueous binding reaction was stopped using magnetic separation. The protein-bead complex was then washed three times via the following protocol: resuspension in 200 µL selection buffer (1× SB; 50 mM HEPES, 150 mM NaCl, 6 mM KCl, 2.5 mM MgCl₂, 2.5 mM CaCl₂, 0.01% Tween-20, pH 7.4), mix by pipetting, pellet beads via magnetic separation, remove supernatant. The washed bead-protein complex was finally resuspended with an additional 100 µL selection buffer and stored at 4°C before use.

Selection of dual random domain DNA aptamers

Aptamer selection was carried out by using magnetic bead-based methods. First, the DNA library was diluted in water and selection buffer (1× SB) and heated at 90°C for 3 minutes, followed by annealing at room temperature (RT, 23°C) for 5 minutes. Then, the storage buffer of the BA.5 S protein-conjugated magnetic beads was removed, and the protein-beads were washed once with 1× SB (0.5 mL). The DNA library solution was mixed with the protein-bead pellet, and the selection reaction was incubated at RT for 2 hours, shaking at 900 rpm. After washing

three times with $1 \times SB$, the magnetic bead pellets were resuspended with 50 μ L of $1 \times SB$ and heated at 90°C for 10 minutes. The 50 μ L of supernatant was collected for PCR1, by adding 1× Tag buffer (50 μL, 50 mM KCl, 10 mM Tris-HCl, 1.5 mM MgCl₂, 1% v/v Triton X-100, pH 9.0), forward primer (25 µL, 10 µM), reverse primer (25 µL, 10 µM), Taq DNA polymerase (5 uL, 5 U/uL), dNTP (10 μL, 10 mM), and ddH₂O (335 μL). PCR1 was carried out using the following temperature profile: preheating at 94°C for 30 s; thermo cycles of 94°C for 30 s, 50°C for 30 s, and 72°C for 30 s; annealing at 72°C for 5 min. Afterwards, the PCR1 product was utilized as the template for PCR2. The PCR2 mixture was prepared by mixing the PCR1 product (100 μ L), forward primer (50 μ L, 10 μ M), reverse primer (50 μ L, 10 μ M), 10× Tag buffer (100 μ L), Taq DNA polymerase (10 μ L, 5 U/ μ L), dNTP (20 μ L, 10 mM), and ddH₂O (670 μ L). The amplification reaction used the same temperature profile as PCR1. Following amplification, ethanol precipitation was performed with the PCR1 product to concentrate and desalt the DNA. Briefly, the PCR2 product (1 mL) was mixed with NaOAc buffer (100 µL, 3 M, pH 5.2) and ethanol (2.5 mL, -20°C), and pelleted by centrifugation at 15,000 rpm for 20 min. The pellet was washed once with 70% v/v ethanol (2.5 mL, -20°C) after discarding the supernatant. The DNA pellet was resuspended in water and the aptamer coding strand was purified by 10% urea denaturing polyacrylamide gel electrophoresis (PAGE). The gel band was visualized using the UV-shadow method, and the sense strand was cut out, and eluted using elution buffer (700 μL, 200 mM NaCl, 10 mM Tris, 1 mM EDTA, pH 7.5). Ethanol precipitation was repeated, as described above, and the enriched library was quantified by UV-Vis absorbance at 260 nm for the next round. A total of 16 rounds were completed.

Selected enriched DNA library pools were amplified by PCR using primers with sequencing tags and then analyzed using the MiSeq (Illumina) sequencing platform using our previously published protocols.^[62]

2.3. Characterization of dual random domain aptamer binding

Radiolabelling of DRD aptamers and enriched DNA library pools

DRD aptamers and DNA library pools were labeled with γ -[32 P] ATP at the 5'-end using PNK reactions according to the manufacturer's protocol. As a summary, 2 μ L of 1 μ M DNA aptamers were mixed with 2 μ L of γ -[32 P] ATP, 1 μ L of 10 x PNK reaction buffer A, 10 U (U: unit) of PNK and 4 μ L water. The mixture was incubated at 37 °C for 20 minutes, purified by 10% denaturing PAGE, and finally concentrated using ethanol precipitation.

Dot blot binding assays of DRD aptamers and enriched DNA library pools with Omicron BA.5 S protein

Dot blot assays were performed using a Whatman Minifold-1 96-well apparatus and a vacuum pump (**Figure 2.1A**). Before experiments, nitrocellulose membranes and nylon membranes were incubated in dot blot binding buffer (1× SB) for 1 hour. γ -[³²P] labelled DRD aptamers or DNA pools (1 nM) were dissolved in the binding buffer and heated at 90 °C for 5 minutes, and then cooled at room temperature for 20 min. Omicron BA.5 S protein was dissolved and diluted in the same buffer. 5 μ L of the above aptamer solution was mixed with 15 μ L of spike protein with different concentrations. The mixture was incubated at room temperature for 1 hour. The dot blot apparatus was assembled with a nitrocellulose membrane on the top, a nylon membrane in the middle, and a wetted Whatman paper in the bottom. After washing each well

18

with 100 μ L of binding buffer, the binding mixtures were loaded and drained by the vacuum pump (force: 550 mmHg for 8 seconds). The wells were then washed twice with 100 μ L binding buffer. The membranes were imaged using a Typhoon 9200 imager (GE Healthcare) and analyzed using Image J software.

Each binding assay was performed two times. The bound fraction (membrane-bound fraction) was quantified and plotted against the concentration of the protein. The K_d values were derived via curve fitting using Origin 8.0 using the equation: $Y = B_{\text{max}}Y/K_d + X$) (Y is the bound fraction of the aptamer with protein, B_{max} is the maximum bound fraction of aptamer, and X is the protein concentration).

Dot blot binding assays of DRD aptamers with Omicron BA.5 Pseudotyped Lentiviruses

Dot blot assays with Omicron BA.5 SARS-CoV-2 spike-pseudotyped lentivirus and the control lentivirus were performed similarly to the procedure as described above except: the aptamer solution was diluted 1:10, and the aptamer solutions were incubated with different concentrations of virus (0 - 900 fM) of viral particles for 10 minutes rather than 1 hour.

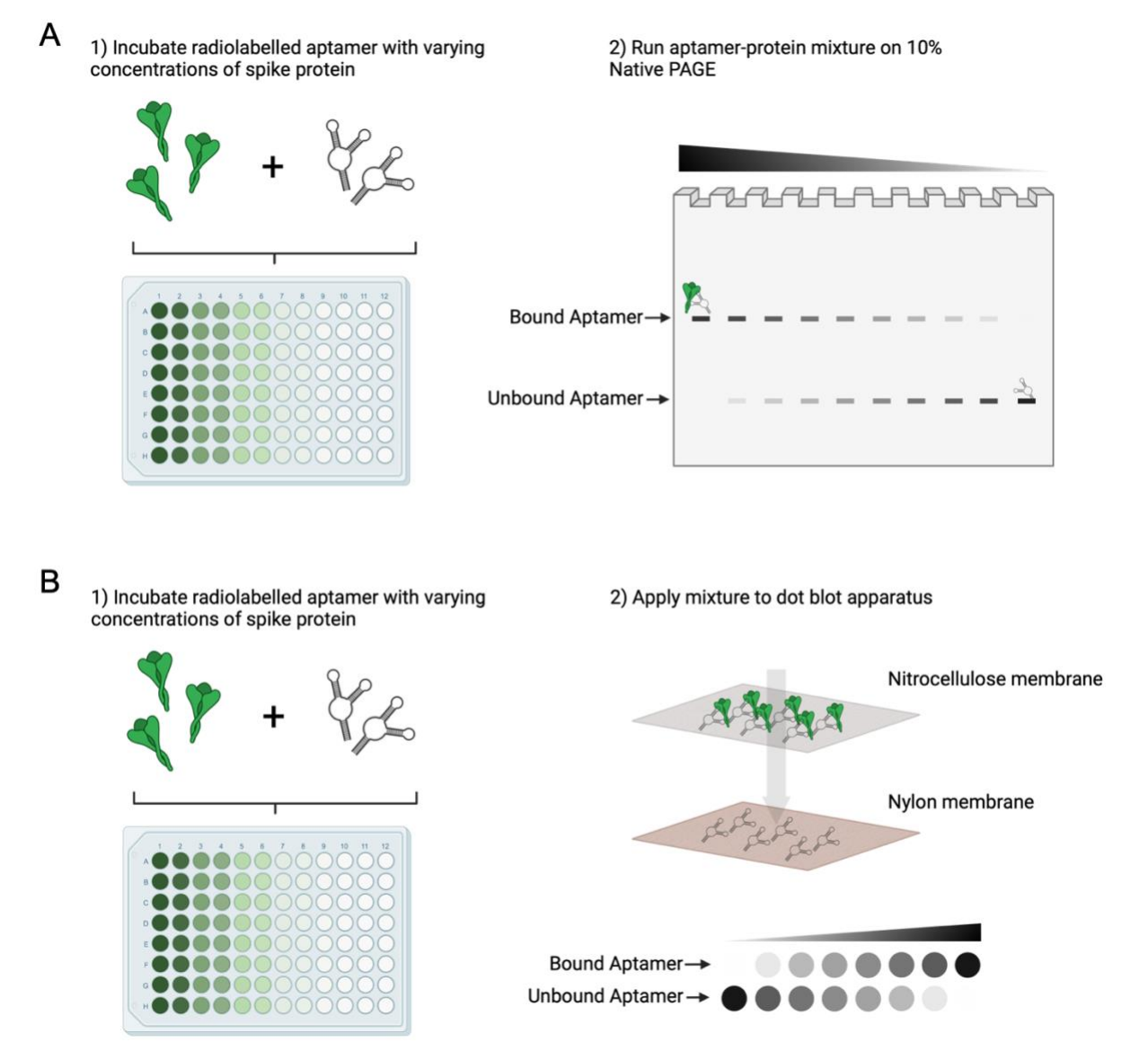


Figure 2.1. Illustration of electromobility shift assay (EMSA) and dot blot assay for characterization of aptamer binding. Both assays begin by incubating radiolabelled aptamer with varying concentrations of spike protein for 1 hour. In EMSA experiments (A), these mixtures are run on a 10% native PAGE to separate bound and unbound fractions. In dot blot assays (B), the bound fractions are retained on the nitrocellulose membrane and unbound fractions flow to the nylon membrane. After each experiment, the gel or membranes are exposed to a storage phosphor screen and imaged.

Electrophoretic mobility shift assays (EMSA) of DRD aptamers and enriched DNA library pools with Omicron BA.5 S protein

The binding of DRD aptamers and DNA pools with Omicron BA.5 S protein was tested by an electrophoretic mobility shift assay (EMSA) (**Figure 2.1B**). The γ -[\$^{32}P] labelled DRD aptamers or DNA pools (1 nM) were dissolved in the binding buffer and heated at 90 °C for 5 minutes, and then cooled at room temperature for 20 min. Omicron BA.5 S protein was dissolved and diluted in the same buffer. 5 μ L of the above aptamer solution was mixed with 15 μ L of spike protein with different concentrations. The mixture was incubated at room temperature for 1 hour. The samples were analyzed using miniature 10% native PAGE via the Bio-Rad Mini-PROTEAN Tetra Cell apparatus, running the gel for 20 min at 100 V. The gels were imaged using a Typhoon 9200 imager (GE Healthcare) and analyzed using Image J software.

CHAPTER 3: DRD APTAMER SELECTION AGAINST SARS-COV-2 OMICRON BA.5 SPIKE PROTEIN

3.1. Rationale of dual random domain library design

The DNA library was designed with two 25-nucleotide fully randomized regions between a 20-nucleotide poly-T linker. The library design was based on the library utilized in the lab's first aptamer selection for SARS-CoV-2. The unique feature of the library is that the flanking primers create a stable hairpin stem. This was done for two reasons: (1) to ensure that the primers do not play an important role in target binding, and (2) to emulate many other high-affinity DNA aptamers, which also possess hairpin stems. [63–65] Regarding the poly-T linker, a 20-nucleotide length was used because our previous S protein dimeric aptamer research show that 20 nucleotides is the shortest possible linker length with no detriment to its binding affinity. [35] Finally, each random region was chosen to consist of 25 nucleotides to preserve enough sequence space for adequate interaction with the target. Magnetic bead-based selection was used to isolate aptamers from the library. Histidine tagged trimeric S protein of the Omicron BA.5 subvariant of SARS-CoV-2 was conjugated onto Ni-NTA modified magnetic beads. BA.5 S protein was chosen as the selection target because it was the latest available protein of the Omicron subvariant at the time.

The dual random domain aptamer library was incubated with the BA.5 S protein-conjugated beads to allow binding. Unbound sequences were removed through washing, and the bound sequences were amplified via PCR to generate an enriched pool for the following round. Specifically, two sets of PCR were conducted per round. The first sets were completed with the forward primer and reverse primer. The second sets were instead completed with the forward primer and reverse blocked primer, which contains the sequence of the reverse primer as well as

a non-amplifiable hexa-ethylene glycol linker. This design allowed us to achieve ssDNA regeneration after running the PCR products on a denaturing PAGE.

The selection pressure was gradually increased to create more stringent conditions by decreasing the amount of protein and library (**Table S2**). More specifically, the selection began with 10000 nM of DNA library and 4000 nM of S protein. Most of the following rounds, with the exception of rounds 4-6 and 10-12, had a near 2-fold reduction in concentration to push the binding constant of the selection to as low as possible. A total of 16 rounds of selection were completed.

Throughout the selection, the binding affinity of the library pools of rounds 0, 6, 8, 10, 12, 14, and 16 were evaluated by EMSA. The DNA libraries were labelled with ^{32}P at the 5' end, and then incubated with the Omicron BA.5 S protein to allow potential binding to occur. Aptamer-protein solutions were then loaded onto a 10% native PAGE to allow for separation of the aptamer-target complexes and the γ -[^{32}P] labelled DNA sequences. In principle, the DNA-protein complexes are larger and move slower on a nondenaturing PAGE, in comparison to unbound DNA.[66] The aptamer bound fraction, as a function of the target protein concentration, was plotted to derive corresponding K_d values. The EMSAs shown in **Figure S1** confirmed that the selection was successful, in that the enriched pools were binding to the S protein. Of importance was the significant jump in binding affinity from round 6 (14 nM) to round 8 (1.4 nM), likely attributed to the increased selection stringency. An increase was also observed for later pools, but the level of binding plateaued in later rounds, with K_d values ranging between 0.1-0.6 nM for the enriched pools of round 10-16.

3.2 Deep sequencing of DNA pools

High-throughput sequencing was then completed with all 16 pools using a previously described protocol. [62] Sequencing tags compatible with the library primers were obtained. Each selection round involved preparing twenty PCR reactions using a 1:20-diluted PCR-1 product stock as the template. After PCR, samples were separated on a 3% agarose gel at 100 volts for 30 minutes. Gel bands containing DNA were excised and purified using the Monarch® Gel Extraction Kit (NEB). The purified samples were then quantified and submitted for sequencing.

The top 50 unique sequences are listed in **Table S3**. These 50 sequences were then sorted into 14 different classes of sequences (**Table S4**) that share the same left (**Table S5**) and right (**Table S6**) domain. The aptamers are named DRDAX, where DRDA stands for <u>Dual Random Domain Aptamer</u>, and X is the numeral that represents the ranking of the unique aptamer sequence in the round 16 pool.

CHAPTER 4: DRD APTAMER CHARACTERIZATION

4.1. Assessment of binding affinity of top 5 aptamer classes for BA.5 S protein

Typically, following an aptamer selection, the top-ranking unique sequences from the final round pool are tested for their affinity. However, in our round 16 pool, the top 50 ranking individual sequences shared great similarity with differences only in the poly-T linker length. We therefore organized these 50 sequences into 14 different classes of sequences that share the same left and right binding domain (**Table S4**). We decided to test the top 5 classes, and we used the most populous sequence of that class as its representative. Accordingly, for class 1, 2, 3, 4, and 5, we tested DRDA-1, -3, -5, -8, and -10, respectively.

The binding affinity of these 5 aptamers were measured using the standard dot blot assays, a common and simple technique used to test the affinity of DNA-protein interactions.^[67–69] **Figure S2A** displays a representative dot blot assay for DRDA-1 and DRDA-8, and **Figure S2B** presents the corresponding binding curves used to derive the K_d values. All five aptamers demonstrated excellent binding affinity, with K_d values below 1 nM. DRDA-8 and DRDA-10 produced the highest binding affinity ($K_d = 0.15$ nM) among these aptamers (**Figure 4.1**). DRDA-8 and DRDA-10 were therefore chosen for any further characterization assays.

To determine how our DRD aptamers rank compared to our previous monomeric (MSA52) and dimeric (DSA52) aptamer for the SARS-CoV-2 S protein, we conducted a binding assessment comparison. DRDA-8 and DRDA-10 show a much higher affinity over MSA52 and DSA52 for the BA.5 S protein, with a K_d value that is 17-fold lower than MSA52 and 3-fold lower than DSA52 (**Figure S2C**). Thus, using the DRD library approach, we could successfully generate aptamers with dimeric-like affinity for the S-protein in a single selection.

25

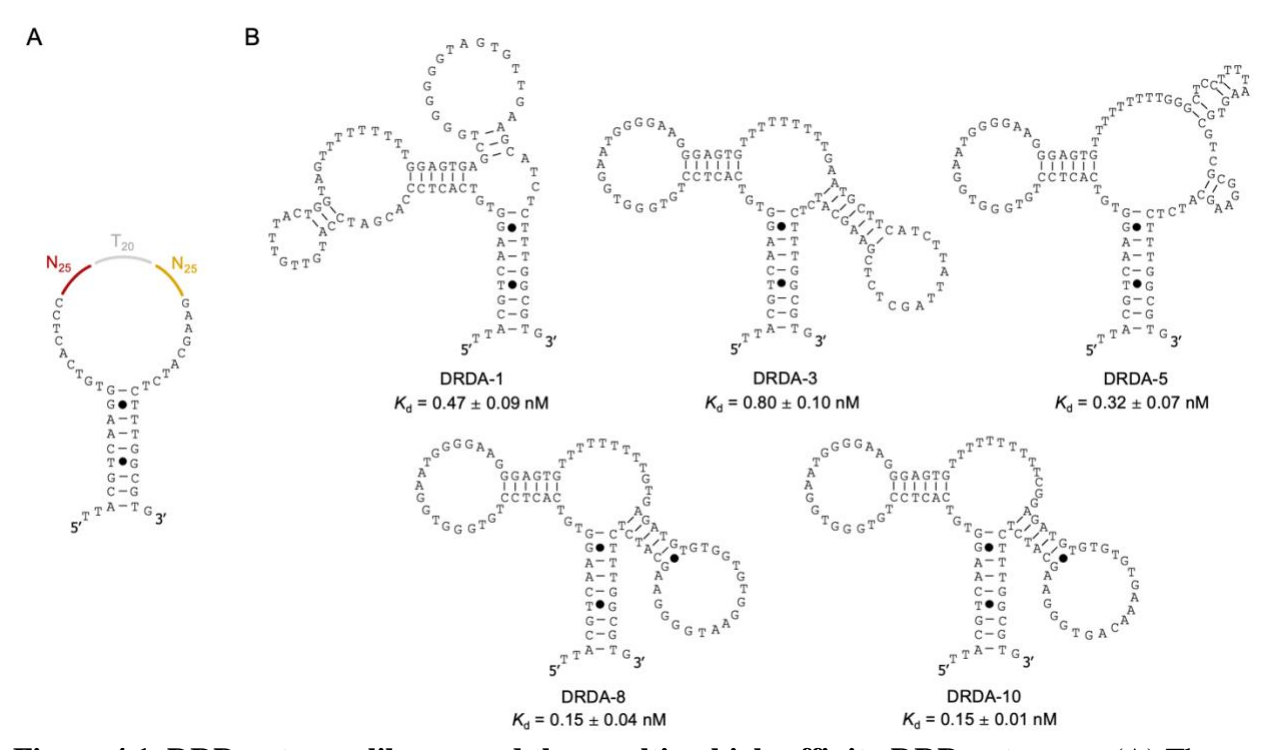


Figure 4.1. DRD aptamer library and the resulting high-affinity DRD aptamers. (A) The secondary structure of the pre-engineered DNA library, containing a 20-nt Poly-T linker between two 25-nt random regions. (B) The secondary structure of the representative aptamer for the top 5 classes (DRDA-1, DRDA-3, DRDA-5, DRDA-8, DRDA-10) with their respective K_d values.

4.2. Binding of a pseudotyped Omicron BA.5 SARS-CoV-2 lentivirus by DRDA-8 and DRDA-10

We then tested the binding of DRDA-8 and DRDA-10 to pseudotyped lentiviruses (PV) expressing the Omicron BA.5 spike protein. As mentioned in our previous papers, these lentiviruses resemble that of SARS-CoV-2 but cannot replicate themselves beyond cell entry; they are, therefore, a safe and adequate substitute for SARS-CoV-2. [70] Each viral particle of SARS-CoV-2 carries multiple trimeric S proteins, and thus, an enhanced affinity can be expected. The same lentivirus that lacks the Omicron BA.5 spike proteins on its surface was used as a control (CV). Dot-blot assays were once again used to measure the affinity against the PV and CV, and the results are presented in **Figure 4.2**. Both DRD aptamers could bind and recognize the PV, but did not demonstrate any binding to the CV. The K_d values of DRDA-8 and DRDA-10 for the PV are 2.8 fM and 4.3 fM, respectively. If we compare this approximation to our previous dimeric aptamer for the SARS-CoV-2 S protein, which had a binding affinity for PV in the low pM range, [35] we can conclude that the DRD aptamers once again possess an affinity that exceeds our previous dimeric aptamers.

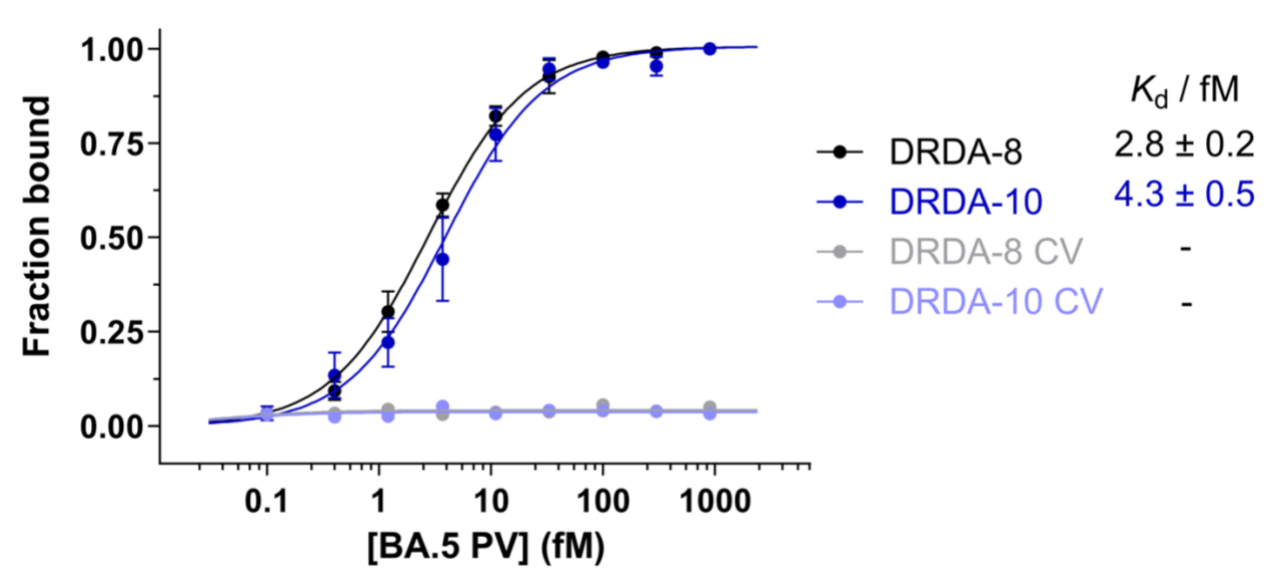


Figure 4.2. Assessment of binding affinity of DRDA-8 and DRDA-10 to pseudotyped lentiviruses (PV) engineered to display the Omicron BA.5 S protein of SARS-CoV-2. Binding curves used to determine K_d values for DRD aptamers. CV: lentivirus that lacks the S protein. An estimated 100 pM of labelled DNA aptamer was incubated with BA.5 S protein of concentrations ranging from 900-0.1 fM for 10 minutes. Following incubation, the aptamer-protein mixtures were subjected through dot blot filtration and the membranes were subsequently imaged. Bound fractions were quantified and plotted to obtain K_d values.

4.3. Multivalent characterization of DRDA-8 and DRDA-10

After confirming the "dimeric-like" affinity of DRD aptamers for the S protein and the pseudovirus, the next logical step was to validate whether these aptamers possessed characteristics similar to typical dimeric aptamers. We began by analyzing the secondary structure of DRDA-8 and DRDA-10, which was predicted by mfold. Each aptamer contains 3 paired elements (P1, P2, P3) and 3 unpaired elements (L1, SS23, L2). Interestingly, the folded elements produce a structure that resembles a dimeric, dual-arm shape, where each random region is clearly defined by its own monomeric stem and loop structure.

If the DRD aptamers were to act like dimeric aptamers, we hypothesized that the affinity of each individual binding arm on its own would show a significant reduction in affinity when compared to the full-length structure with two arms. To test this, several truncated mutants of DRDA-8 were analyzed via dot blot assay for the binding activity to the Omicron BA.5 S protein (**Figure 4.3A**). Truncation 1 has the structural elements of the first binding arm removed (P2, L1), Truncation 2 has the structural elements of the second binding arm removed (P3, L2), and Truncation 3 has both binding arms removed (P2, P3, L1, L2). In Truncation 1 and Truncation 2, a near 10-fold loss in binding activity is observed (Truncation 1: $K_d = 1.3$ nM, Truncation 2: 1.2 nM) when compared to the full-length aptamer ($K_d = 0.15$ nM). Truncation 3 suffers an even greater loss in activity, with no binding observed at concentrations lower than 10 nM. These results suggest that both random regions and binding arms are imperative, and they work in cohesion to provide better avidity and affinity to the target, similar to any other dimeric aptamer.

Although not related to the binding arms, the hairpin primers (P1) were also analyzed in Truncation 4 and Truncation 5, with a partial and complete removal, respectively (**Figure S3**). In both truncated mutants, the binding activity is still retained (Truncation 4: $K_d = 0.25 \pm 0.09$ nM,

Truncation 5: 0.12 ± 0.03 nM), suggesting that the primers play no major role in target recognition. The same five truncations were performed against DRDA-10, and similar trends were observed with the binding arms and hairpin primers (**Figure 4.3B, Figure S4**).

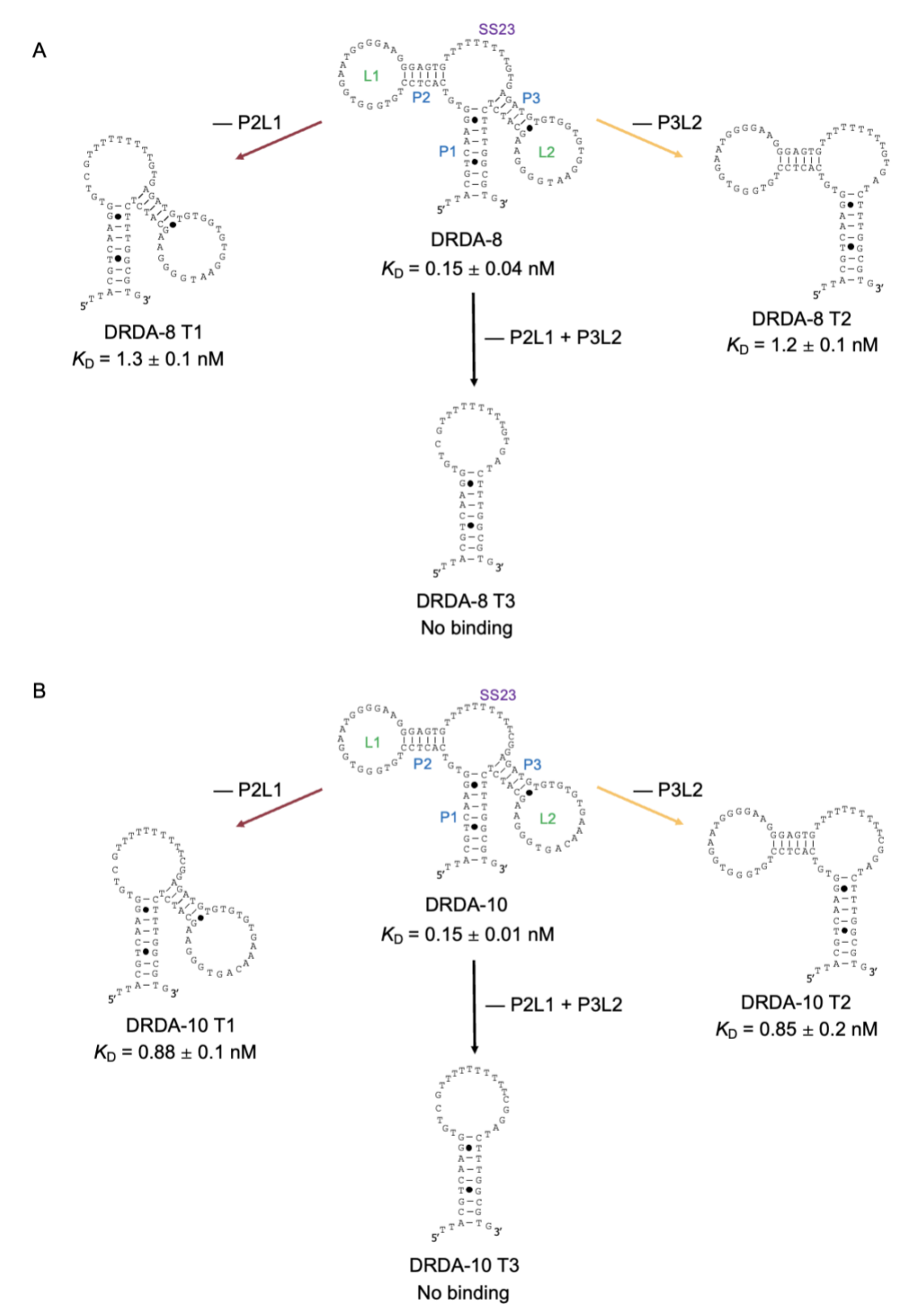


Figure 4.3. Truncation analysis of DRDA-8 and DRDA-10. (A) Secondary structure of DRDA-8 and the binding affinity of the full-length aptamer and truncations 1-3. (B) Secondary structure of DRDA-10 and the binding affinity of the full-length aptamer and truncations 1-3.

To further test the dimeric binding performance of the DRD aptamers, another binding assay was conducted. In the experiment, two DRDA-8 mutants were generated with the loop sequences of either binding arm scrambled (L1 Scramble, L2 scramble). The binding of these sequences to the Omicron BA.5 S protein was then analyzed via dot blot analysis (**Figure S5**). Similar to the truncation assays, a clear reduction in affinity is observed when one of the two loops are scrambled. Taken together, the truncation and scramble sequence assessments suggest that the two arms in DRDA-8 and DRDA-10 act synergistically for target recognition, similar to how other high-performing dimeric aptamers operate.

Another important area of investigation was to assess whether the DRD aptamers were behaving similar to heterodimers or homodimers. [33] Heterodimers, composed of different aptamer ligands, typically recognize distinct epitopes on a multimeric protein. On the other hand, homodimers, which are composed of the same two aptamer ligands, will recognize and bind to the same epitope on differing subunits. To test whether each binding arm recognized a distinct epitope on the Omicron BA.5 S protein, we conducted a competition assay that used non-radioactive DRDA-8 Truncation 2 to compete with radioactive DRDA-8 Truncation 1. We first incubated radioactive DRDA-8 Truncation 1 under the condition that Truncation 1 was nearfully bound to the S protein. Then, non-radioactive DRDA-8 Truncation 2 was added at varying concentrations to allow for competition. The results in **Figure 4.4** indicate that Truncation 2 will compete with Truncation 1. Initially, Truncation 1 binds tightly to the S protein at relatively low amounts of competing Truncation 2. However, as the concentration of Truncation 2 increases to approximately 50 nM, radiolabeled Truncation 1 is clearly outcompeted by non-labeled Truncation 2.

The reverse assay with labelled Truncation 2 and non-labelled Truncation 1 is provided in **Figure 4.5**. Competition at higher competing aptamer concentrations was observed once again. Overall, these results suggest that the two arms of DRDA-8 are more likely acting as homodimers, recognizing the same epitopes on differing subunits of the trimeric S protein.

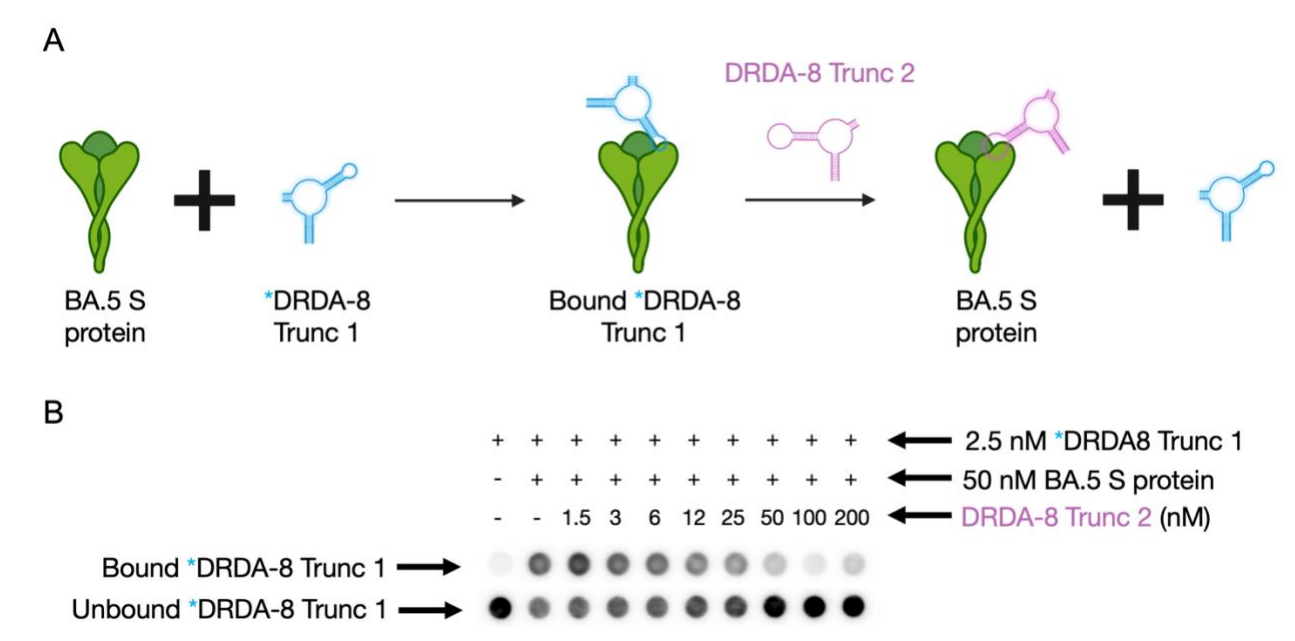


Figure 4.4. Competition between DRDA-8 Truncation 1 and DRDA-8 Truncation 2 for binding to the S protein. A) Assay schematic. Radioactive Truncation 1 is allowed to bind fully to BA.5 S protein before competition with Truncation 2. (B) Assay results. A 50 nM solution of BA.5 S protein was incubated with 2.5 nM radioactive (*) Truncation 1, followed by the addition of 1.5-200 nM non-radioactive Truncation 2.

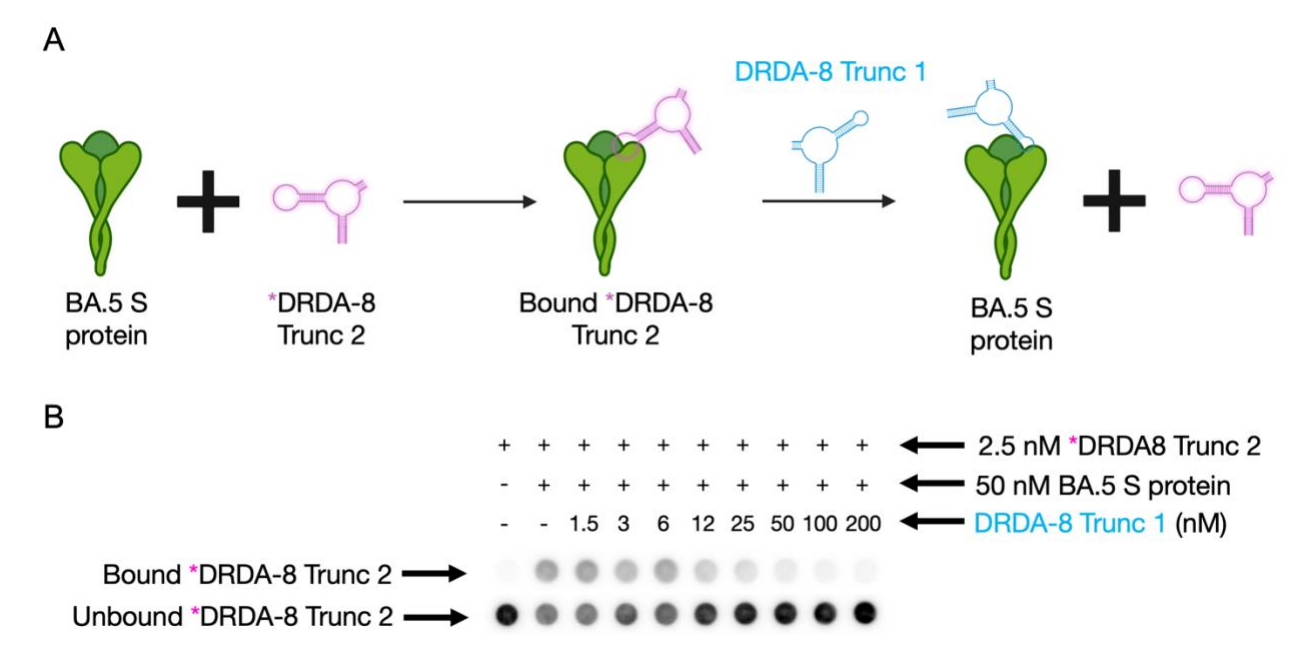


Figure 4.5. Competition between DRDA-8 Truncation 2 and DRDA-8 Truncation 1 for binding to the S protein. A) Assay schematic. Radioactive Truncation 2 is allowed to bind fully to BA.5 S protein before competition with Truncation 1. (B) Assay results. A 50 nM solution of BA.5 S protein was incubated with 2.5 nM radioactive (*) Truncation 2, followed by the addition of 1.5-200 nM non-radioactive Truncation 1.

4.4. T-linker shortening analysis

One of the more interesting phenomena from the selection was that the poly-T linker, which was initially designed as 20 nucleotides in the library, gradually decreased to 10 nucleotides in the final selection round (**Figure 4.6A**). Our initial assumption was that this was due to a PCR bias, where shorter sequences with deletion mutations were favoured by PCR and were amplified at a higher rate than the longer sequences.^[71] However, we also considered that this reduction in length could also be evolutionarily driven, where the aptamers preferred a specific T-linker length for a certain distance and angle between the two binding interactions against the S protein. To investigate this hypothesis, the affinity of four DRDA-8 mutants were tested in which the poly-T linker was either shortened to 5 nucleotides or extended to 20, 30, or 40 nucleotides (**Figure 4.6B**). The results indicate that the extension or shortening of the linker does not significantly improve the binding affinity. The K_d value of the original DRDA-8 aptamer is 0.15 nM, while those of the T-linker mutants range from 0.08 to 0.29 nM. Therefore, the trend observed with the poly-T linker likely represents a simple PCR bias rather than any evolutionary change.

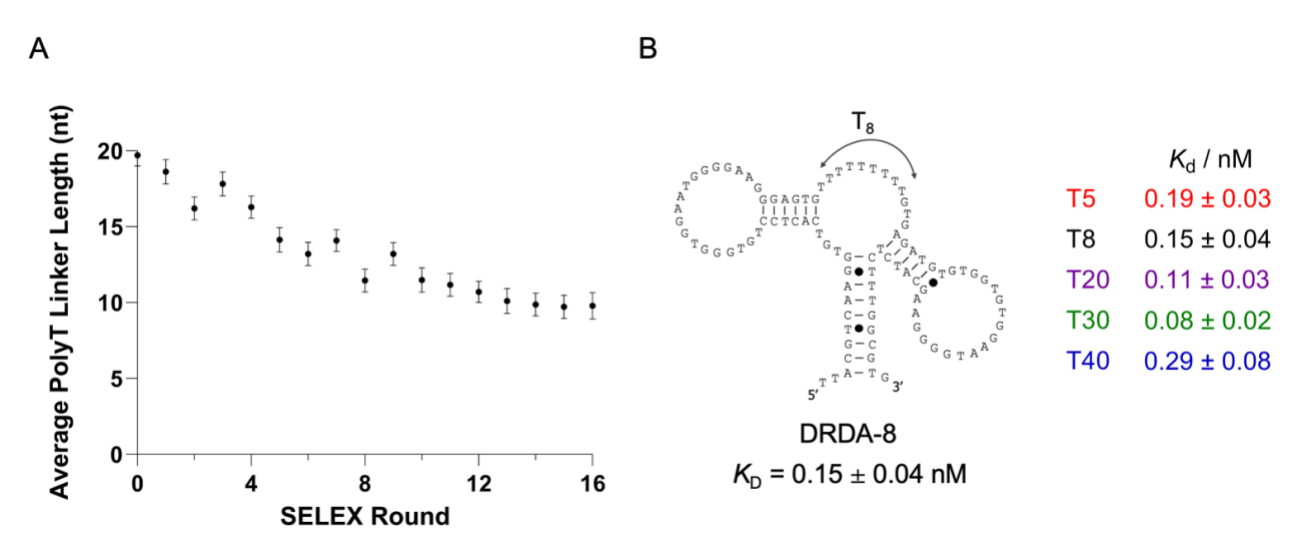


Figure 4.6. DRD aptamer poly-T linker analysis. (A) Trend of average poly-T linker length from round 0 to round 16. Linker length decreased from an average of 19.5 nucleotides to 9.8 nucleotides. (B) Binding affinity of wildtype DRDA-8 and its mutants with extended or shortened T-linker lengths.

4.5. Selectivity assessment of DRDA-8 and DRDA-10

We then finally tested the specificity of DRDA-8 and DRDA-10 by assessing the binding to control proteins. First, three protein targets non-related to SARS-CoV-2 were tested: bovine serum albumin (BSA), human α-thrombin, and human immunoglobulin G (IgG). BSA and IgG were chosen since they are commonly used as control proteins in biochemical assays, while thrombin was chosen as it is a popular aptamer target in the literature. **Figure 4.7A** and **4.7B** show the dot blot results for DRDA-8 and DRDA-10, respectively. A non-protein (i.e., buffer only) lane was used as a negative control, and the Omicron BA.5 S protein was used as a positive control. The results of the dot blot clearly indicate that neither DRD aptamer shows binding to the three non-related control proteins.

On the same assay, DRDA-8 and DRDA-10 were then tested against several proteins that have varying similarity to the SARS-CoV-2 S protein. These included the S protein of SARS-CoV-1 and MERS, the receptor-binding domain (RBD) of four different seasonal coronaviruses (HKU1, 229E, NL63, OC43), and the hemagglutinin A protein of the CAL 09 influenza strain. Minimal binding was observed for DRDA-8 against the MERS S protein, which shares around 50% sequence similarity with the SARS-CoV-2 genome. However, this virus is no longer in circulation, in contrast to the seasonal coronaviruses. Aside from this binding, no cross-reactivity was observed with the other proteins, proving that the DRD library strategy can also generate aptamers with high specificity.

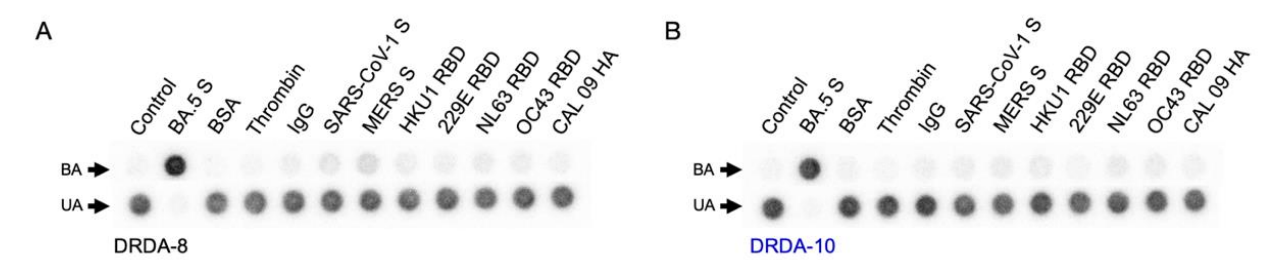


Figure 4.7. **Selectivity assessment of DRDA-8 and DRDA-10.** Dot blot results of (A) DRDA-8 and (B) DRDA-10 for binding to the S protein of the SARS-CoV-2 Omicron BA.5 variant and control proteins including BSA, thrombin, the spike proteins of SARS-CoV-1 and MERS, the RBD of four seasonal coronaviruses (HKU1, 229E, NL63, OC43), and the hemagglutinin (HA) protein of the A/California/04/2009 (CAL 09) influenza strain.

CHAPTER 5: CONCLUSION AND FUTURE DIRECTIONS

In summary, we have presented a dual random domain aptamer library strategy that directly selects for "dimeric-like" aptamers. The DRD library takes inspiration from our previous dimeric aptamers for COVID-19, which had two 40-nt aptamers connected with a 20-nt poly-T linker. Similarly, our library also contains a 20-nt poly-T linker but contains two 25-nt random regions. In selecting for two random regions separately and providing them enough distance to form their individual binding moieties, we were able to obtain "dimeric-like" aptamers in a single selection. Sixteen total rounds were completed, and the two best aptamers (DRDA-8 and DRDA-10) displayed a binding affinity that outperformed our previous monomeric and dimeric aptamers for the SARS-CoV-2 spike protein. In fact, in comparison to other published aptamers that have been directly selected for SARS-CoV-2 (i.e., excluding those that have been engineered post-selection), DRDA-8 and DRDA-10 are the current highest-affinity aptamers for the S-protein (Table S7). nCoV-S1-Apt1 selected by Yang *et al.* possesses a *K*_d value of 0.3 nM for the S1 protein, and the DRD aptamers exceed that by 2-fold for binding to the trimeric S-protein. [73,74]

In testing for its dimeric qualities, we conducted two tests, which included (1) truncation assays, and (2) scramble sequence testing. The assays suggest that both binding arms are critical for target recognition, and they are likely working synergistically to provide a high binding affinity for the S-protein. We also ran a competition assay to determine whether DRDA-8 was behaving like a homodimer or a heterodimer. The clear competition in each assay suggests that the arms likely recognize the same epitope on an individual S protein subunit.

One limitation of the study is that each of these characterization tests relied on the 2-dimensional secondary structure from a computer model (mFold).^[75] These structures can often be misleading given that the minimal free energy structure was assumed and that these aptamers

can take on different conformations. Additionally, secondary structure predictions frequently illustrate the single-stranded binding site as a circular region that interacts with its targets. Yet, this representation can also be misrepresentative due to the three-dimensional intricacies involved in aptamer recognition and binding.^[25] Therefore, the conclusions of the dimeric qualities of the DRD aptamers may be misinterpreted.

Nonetheless, the DRD library strategy provides an interesting strategy for future aptamer selections. Our novel DNA library is capable of generating practical, high-affinity dimeric aptamers in a short turnaround time. This archivable platform may prove useful in situations such as future pandemics when molecular recognition elements for diagnostics and therapeutics are rapidly required.

SUPPLEMENTAL INFORMATION

Table S1. All synthetic oligonucleotides utilized in this study. Sequences are written 5' to 3'. Abbreviations include: N_{25} : 25-nucleotide random region; T_{20} : 20-nucleotide polythymidine linker.

mikei.			Select	ion			
DNA Library	(109 nt)	TTACGTCAAGGTGTCACTCC-N ₂₅ -T ₂₀ -N ₂₅ -GAAGCATCTCTTTGGCGTG					
Forward Primer (20 nt)		TTACGTCAAGGTGTCACTCC TTACGTCAAGGTGTCACTCC					
Reverse Primer (19 nt)		CACGCCAAAGATGCTTC					
Reverse Blocked				LSP18/CACGC	TAAAGAGATGC'	рψС	
Primer (39 nt)	cu			101 107 0110000	211111011011100		
Time (39 m)			Aptan	AOPC .			
Name	Size	Ι	Aptan	1618			
Name	(nt)						
DRDA-1	97	TTACGTCAAG	GTGTCACTCC	CACGATCCAT	GTTGTTTACT	GGTAGTTTTT	
DRDITT				GTAGTGTTGA			
DRDA-2	98			CACGATCCAT			
DRDIT 2	70			GGTAGTGTTG			
DRDA-3	97			TGTGGGTGGA			
DRDIT 3				TAGCTCTCGA			
DRDA-4	96			CACGATCCAT			
DRD/1				TAGTGTTGAA			
DRDA-5	96			TGTGGGTGGA			
DRDIT 3	70			CGTCGCGGAA			
DRDA-6	97			TGTGGGTGGA			
DRD/1 0				GCGTCGCGGA			
DRDA-7	98			TGTGGGTGGA			
DIEDIT /				TTAGCTCTCG			
DRDA-8	97			TGTGGGTGGA			
DIEDITO				GGAATGGGGA			
DRDA-9	98			TGTGGGTGGA			
2112117				TTAGCTCTCG			
DRDA-10	99			TGTGGGTGGA			
21121110		TTTTTCGGAG	ATGTGTGTGT	GAAACAGTGG	GAAGCATCTC	TTTGGCGTG	
DRDA-8	68	TTACGTCAAG	GTGTCGTTTT	TTTTTGTGAG	ATGTGTGGTG	TGGAATGGGG	
Truncation 1		AAGCATCTCT	TTGGCGTG				
DRDA-8	69	TTACGTCAAG	GTGTCACTCC	TGTGGGTGGA	ATGGGGAAGG	GAGTGTTTTT	
Truncation 2		TTTTGTGATC	TTTGGCGTG				
DRDA-8	40	TTACGTCAAG	GTGTCGTTTT	TTTTTGTGAT	CTTTGGCGTG		
Truncation 3							
DRDA-8	84	AAGGTGTCAC	TCCTGTGGGT	GGAATGGGGA	AGGGAGTGTT	TTTTTTTGTG	
Truncation 4		AGATGTGTGG	TGTGGAATGG	GGAAGCATCT	CTTT		
DRDA-8	78	GTGTCACTCC	TGTGGGTGGA	ATGGGGAAGG	GAGTGTTTTT	TTTTGTGAGA	
Truncation 5		TGTGTGGTGT	GGAATGGGGA	AGCATCTC			
DRDA-10	70	TTACGTCAAG	GTGTCGTTTT	TTTTTTCGGA	GATGTGTGTG	TGAAACAGTG	
Truncation 1			CTTTGGCGTG	-			
DRDA-10	70	TTACGTCAAG	GTGTCACTCC	TGTGGGTGGA	ATGGGGAAGG	GAGTGTTTTT	
Truncation 2		TTTTTCGGAT	CTTTGGCGTG				
DRDA-10	41	TTACGTCAAG	GTGTCGTTTT	TTTTTTCGGA	TCTTTGGCGT	G	
Truncation 3				-			
DRDA-10	86	AAGGTGTCAC	TCCTGTGGGT	GGAATGGGGA	AGGGAGTGTT	TTTTTTTCG	
Truncation 4				TGGGAAGCAT			
DRDA-10	80			ATGGGGAAGG		TTTTTCGGAG	
Truncation 5				GAAGCATCTC			
- 1 0110 011 011 0	1	l .					

 $M.Sc.\ Thesis-R.\ Amini; McMaster\ University-Biochemistry\ \&\ Biomedical\ Sciences$

DRDA-8 T5	93	TTACGTCAAG	GTGTCACTCC	TGTGGGTGGA	ATGGGGAAGG	GAGTGTTTTT
	93					
Linker		GTGAGATGTG	TGGTGTGGAA	TGGGGAAGCA	TCTCTTTGGC	GTG
DRDA-8	109	TTACGTCAAG	GTGTCACTCC	TGTGGGTGGA	ATGGGGAAGG	GAGTGTTTTT
T20 Linker		TTTTTTTTTT	TTTTTTGTGA	GATGTGTGGT	GTGGAATGGG	GAAGCATCTC
		TTTGGCGTG				
DRDA-8	119	TTACGTCAAG	GTGTCACTCC	TGTGGGTGGA	ATGGGGAAGG	GAGTGTTTTT
T30 Linker		TTTTTTTTTT	TTTTTTTTT	TTTTTTGTGA	GATGTGTGGT	GTGGAATGGG
		GAAGCATCTC	TTTGGCGTG			
DRDA-8	129	TTACGTCAAG	GTGTCACTCC	TGTGGGTGGA	ATGGGGAAGG	GAGTGTTTTT
T40 Linker		TTTTTTTTTT	TTTTTTTTTT	TTTTTTTTTT	TTTTTTGTGA	GATGTGTGGT
		GTGGAATGGG	GAAGCATCTC	TTTGGCGTG		
MSA52	79	TTACGTCAAG	GTGTCACTCC	GTAGGGTTTG	GCTCCGGGCC	TGGCGTCGGT
		CGTCTCTCGC	GAAGCATCTC	TTTGGCGTG		
DSA52	178	TTACGTCAAG	GTGTCACTCC	GTAGGGTTTG	GCTCCGGGCC	TGGCGTCGGT
		CGTCTCTCGC	GAAGCATCTC	TTTGGCGTGT	$\tt TTTTTTTTTT$	TTTTTTTTT
		TACGTCAAGG	TGTCACTCCG	TAGGGTTTGG	CTCCGGGCCT	GGCGTCGGTC
		GTCTCTCGCG	AAGCATCTCT	TTGGCGTG		
DRDA-8 L1	97	TTACGTCAAG	GTGTCACTCC	GGTGAATTTG	GGGAGGAGGG	GAGTGTTTTT
Scramble		TTTTGTGAGA	TGTGTGGTGT	GGAATGGGGA	AGCATCTCTT	TGGCGTG
DRDA-8 L2	97	TTACGTCAAG	GTGTCACTCC	TGTGGGTGGA	ATGGGGAAGG	GAGTGTTTTT
Scramble		TTTTGTGAGA	TGTGAGGGAT	GAGGTGGGTT	AGCATCTCTT	TGGCGTG

Table S2. Concentrations of DNA and protein used during SELEX.

SELEX Round	DNA Library (nM)	BA.5 Spike Protein (nM)
1	10000	4000
2	1400	800
3	2000	1000
4	800	400
5	800	400
6	800	400
7	400	200
8	200	100
9	100	50
10	50	25
11	50	25
12	50	25
13	25	12.5
14	10	5
15	5	2.5
16	2.5	1.25

Table S3. Top 50 ranking sequences in pool 16 ranked by their percentage.

Rank in pool 16	Sequences (5' – 3')	% in poo 16
Library	NNNNNNNNNNNNNNNNNNNNNNNNNNNNNNNNNNNNNNN	2.7968
1	CACGATCCATGTTGTTTACTGGTAGTTTTTTTTTGGAGTGAGCTGGGGGGGGTAGTGTT	2.7968
2	CACGATCCATGTTGTTTACTGGTAGTTTTTTTTTTGGAGTGAGCTGGGGGGGGTAGTGTT	1.8595
3	TGTGGGTGGAATGGGGAAGGGAGTGTTTTTTTTTG-AATGCTTCATCTTATTAGCTCTC	1.3718
4	CACGATCCATGTTGTTTACTGGTAGTTTTTTTTGGAGTGAGCTGGGGGGGGTAGTGTT	1.2727
5	TGTGGGTGGAATGGGGAAGGGAGTGTTTTTTTTTGGGCTCCTTTTAAGTGCGTCGCG	1.2685
6	TGTGGGTGGAATGGGGAAGGGAGTGTTTTTTTTTTGGGCTCCTTTTAAGTGCGTCGCG	1.2213
7	TGTGGGTGGAATGGGGAAGGGAGTGTTTTTTTTTGTAATGCTTCATCTTATTAGCTCTC	1.0827
8	TGTGGGTGGAATGGGGAAGGGAGTGTTTTTTTTTGTGAGATGTGTGGTGTGGAATGGG	1.0248
9	TGTGGGTGGAATGGGGAAGGGAGTGTTTTTTTTTTG-AATGCTTCATCTTATTAGCTCTC	0.9648
10	TGTGGGTGGAATGGGGAAGGGAGTGTTTTTTTTTTTCGGAGATGTGTGTGTGAAACAGTGG	0.8987
11	TAGTCCTGAGGTGCCCGCGATGGACTTTTTTTTTTCGGAGATGTGTGTGTGAAACAGTGG	0.7954
12	TGTGGGTGGAATGGGGAAGGGAGTGTTTTTTTTTTTGTGAGATGTGTGGTGTGGAATGGG	0.7344
13	TGTGGGTGGAATGGGGAAGGGAGTGTTTTTTTTTCGGAGATGTGTGTGTGAAACAGTGG	0.7240
14	TGTGGGTGGAATGGGGAAGGGAGTGTTTTTTTTTTGTAATGCTTCATCTTATTAGCTCTC	0.6932
15	CACGATCCATGTTGTTTACTGGTAGTTTTTTTTTTTTGGAGTGAGCTGGGGGGGTAGTGTT	0.6830
16	TGTGGGTGGAATGGGGAAGGGAGTGTTTTTTTTTGCCTTCGAATCTTACTAGCTCTCTC	0.6773
17	TAGTCCTGAGGTGCCCGCGATGGACTTTTTTTTTTTCGGAGATGTGTGTGTGAAACAGTGG	0.6750
18	TGTGGGTGGAATGGGGAAGGGAGTGTTTTTTTTTTTTCGGAGATGTGTGTGTGAAACAGTGG	0.6723
19	TGTGGGTGGAATGGGGAAGGGAGTGTTTTTTTTTTTTGGGCTCCTTTTAAGTGCGTCGCG	0.6668
20	TGTGGGTGGAATGGGGAAGGGAGTGTTTTTTTTG-AATGCTTCATCTTATTAGCTCTC	0.5403
21	TAGTCCTGAGGTGCCCGCGATGGACTTTTTTTTTCGGAGATGTGTGTGTGAAACAGTGG	0.5087
22	TGTGGGTGGAATGGGGAAGGGAGTGTTTTTTTTTTGCCTTCGAATCTTACTAGCTCTCTC	0.4930
23	ACATCCGAAGTTGTCCCGAGGTTGTTTTTTTTTGTATGCTTTAAGGGGGTTGTGTC	0.4915
24	ACAGGCGGAGGTGTTCGCGACCCTGTTTTTTTTTGGGGCTTCTAAGGGGGTTGTGTCTG	0.4717
25	CCAGCATCTTATTAGCTCTCGCTGGTTTTTTTTTTCGGGTAAGGGGGTTGTGTCTGCCC	0.4152
26	TGTGGGTGGAATGGGGAAGGGAGTGTTTTTTTTGTAATGCTTCATCTTATTAGCTCTC	0.3979
27	TGTGGGTGGAATGGGGAAGGGAGTGTTTTTTTTTTTTG-AATGCTTCATCTTATTAGCTCTC	0.3852
28	TAGTCCTGAGGTGCCCGCGATGGACTTTTTTTTTTTTTT	0.3802
29	ACAGGCGGAGGTGTTCGCGACCCTGTTTTTTTTTTGGGGCTTCTAAGGGGGTTGTGTCTG	0.3741
30	CCAGCATCTTATTAGCTCTCGCTGGTTTTTTTTTCGGGTAAGGGGGGTTGTGTCTGCCC	0.3675
31	TGTGGGTGGAATGGGGAAGGGAGTGTTTTTTTTGGGCTCCTTTTAAGTGCGTCGCG	0.3658
32	TGTGGGTGGAATGGGGAAGGGAGTGTTTTTTTTTTTTT	0.3655
33	TGTGGGTGGAATGGGGAAGGGAGTGTTTTTTTTGTGAGATGTGTGGTGTGGAATGGG	0.3603
34	TGTGGGTGGAATGGGGAAGGGAGTGTTTTTTTTTTTTGTGAGATGTGTGGTGTGGAATGGG	0.3260
35	AGTGCGTAGCTAAGATGTCTAGCACTTTTTTTTTGGCTTCCTAAGGGGGTTGTGTCTGG	0.3021
36	CCAGCATCTTATTAGCTCTCGCTGGTTTTTTTTTTTTCGGGTAAGGGGGTTGTGTCTGCCC	0.2899
37	TGTGGGTGGAATGGGGAAGGGAGTGTTTTTTTTTTTTGTAATGCTTCATCTTATTAGCTCTC	0.2681
38	ATGTGGGTGGAATGGGGAAGTGGAGTTTTTTTTTCGGAGATGTGTGTGTGAAACAGTGG	0.2492
39	AGTGCGTAGCTAAGATGTCTAGCACTTTTTTTTTTGGCTTCCTAAGGGGGTTGTGTCTGG	0.2481
40	TGTGGGTGGAATGGGGAAGGGAGTGTTTTTTTTTTTTGCCTTCGAATCTTACTAGCTCTCTC	0.2423
41	TGTGGGTGGAATGGGGAAGGGAGTGTTTTTTTTTTTTT	0.2383
42	ACATCCGAAGTTGTCCCGAGGTTGTTTTTTTTGTATGCTTTAAGGGGGTTGTGTC	0.2330
43	TAGTCCTGAGGTGCCCGCGATGGACTTTTTTTTTGGCTTCCTAAGGGGGTTGTGTCTGG	0.2283
44	ACATCCGAAGTTGTCCCGAGGTTGTTTTTTTTTTGTATGCTTTAAGGGGGTTGTGTC	0.2264
45	AGTGCGTAGCTAAGATGTCTAGCACTTTTTTTTTTATGCTGGGGTATATACAGTCTAGAG	0.2243

M.Sc. Thesis – R. Amini; McMaster University – Biochemistry & Biomedical Sciences

46	ACAGGCGGAGGTGTTCGCGACCCTGTTTTTTTTGGGGCTTCTAAGGGGGGTTGTGTCTG	0.2237
47	ATGTGGGTGGAATGGGGAAGTGGAGTTTTTTTTTTCGGAGATGTGTGTGAAACAGTGG	0.2211
48	TGTGGGTGGAATGGGGAAGGGAGTGTTTTTTTTGCCTTCGAATCTTACTAGCTCTCTC	0.2200
49	TAGTCCTGAGGTGCCCGCGATGGACTTTTTTTTTGGCTTCCTAAGGGGGTTGTGTCTGG	0.2048
50	CACGATCGATGTTGTGTACTCGTAGTTTTTTTTTGGAGTGAGCTGGGGGGGTAGTGTT	0.1975

Table S4. Top 50 ranking sequences in pool 16 organized by their class.

Rank in pool 16	Sequences (5' – 3')			
Library	ry NNNNNNNNNNNNNNNNNNNNNNNNNNNNNNNNNNNN			
	Class 1			
1	CACGATCCATGTTGTTTACTGGTAGTTTTTTTTTTT	GGAGTGAGCTGGGGGGGTAGTGTT	2.7858	
2	CACGATCCATGTTGTTTACTGGTAGTTTTTTTTTTTT	GGAGTGAGCTGGGGGGGTAGTGTT	1.8595	
4	CACGATCCATGTTGTTTACTGGTAGTTTTTTTTT	GGAGTGAGCTGGGGGGGTAGTGTT	1.2727	
15	CACGATCCATGTTGTTTACTGGTAGTTTTTTTTTTTTT	GGAGTGAGCTGGGGGGGGTAGTGTT	0.6830	
50	CACGATCGATGTTGTGTACTCGTAGTTTTTTTTTTT	GGAGTGAGCTGGGGGGGGTAGTGTT	0.1975	
			6.7985	
	Class 2			
3	TGTGGGTGGAATGGGGAAGGGAGTGTTTTTTTTT	G-AATGCTTCATCTTATTAGCTCTC	1.3718	
7	TGTGGGTGGAATGGGGAAGGGAGTGTTTTTTTTT	GTAATGCTTCATCTTATTAGCTCTC	1.0827	
9	TGTGGGTGGAATGGGGAAGGGAGTGTTTTTTTTTT	G-AATGCTTCATCTTATTAGCTCTC	0.9648	
14	TGTGGGTGGAATGGGGAAGGGAGTGTTTTTTTTTTT	GTAATGCTTCATCTTATTAGCTCTC	0.6932	
20	TGTGGGTGGAATGGGGAAGGGAGTGTTTTTTTT	G-AATGCTTCATCTTATTAGCTCTC	0.5403	
26	TGTGGGTGGAATGGGGAAGGGAGTGTTTTTTTT	GTAATGCTTCATCTTATTAGCTCTC	0.4152	
27	TGTGGGTGGAATGGGGAAGGGAGTGTTTTTTTTTTT	G-AATGCTTCATCTTATTAGCTCTC	0.3979	
37	TGTGGGTGGAATGGGGAAGGGAGTGTTTTTTTTTTT	GTAATGCTTCATCTTATTAGCTCTC	0.2899	
			5.7558	
	Class 3			
5	TGTGGGTGGAATGGGGAAGGGAGTGTTTTTTTTT	GGGCTCCTTTTAAGTGCGTCGCG	1.2685	
6	TGTGGGTGGAATGGGGAAGGGAGTGTTTTTTTTTTT	GGGCTCCTTTTAAGTGCGTCGCG	1.2213	
19	TGTGGGTGGAATGGGGAAGGGAGTGTTTTTTTTTTTT	GGGCTCCTTTTAAGTGCGTCGCG	0.6668	
31	TGTGGGTGGAATGGGGAAGGGAGTGTTTTTTTT	GGGCTCCTTTTAAGTGCGTCGCG	0.3658	
41	TGTGGGTGGAATGGGGAAGGGAGTGTTTTTTTTTTTTT	GGGCTCCTTTTAAGTGCGTCGCG	0.2383	
			3.7607	
	Class 4		1	
8	TGTGGGTGGAATGGGGAAGGGAGTGTTTTTTTTT	GTGAGATGTGTGTGTGGAATGGG	1.0248	
12	TGTGGGTGGAATGGGGAAGGGAGTGTTTTTTTTTT		0.7344	
33	TGTGGGTGGAATGGGGAAGGGAGTGTTTTTTTT	GTGAGATGTGTGTGTGGAATGGG	0.3603	
34	TGTGGGTGGAATGGGGAAGGGAGTGTTTTTTTTTTTT	GTGAGATGTGTGTGTGGAATGGG	0.3260	
			2.4455	
1.0	Class 5		0.000=	
10	TGTGGGTGGAATGGGGAAGGGAGTGTTTTTTTTTTT		0.8987	
13	TGTGGGTGGAATGGGGAAGGGAGTGTTTTTTTTTTTTT		0.7240	
18	TGTGGGTGGAATGGGGAAGGGAGTGTTTTTTTTTTTTT		0.6723	
32	TGTGGGTGGAATGGGGAAGGGAGTGTTTTTTTTTTTTT	CGGAGATGTGTGTGAAACAGTGG	0.3658	
			2.6608	
1.1	Class 6	000101000000000000000000000000000000000	0.5051	
11	TAGTCCTGAGGTGCCCGCGATGGACTTTTTTTTTTTTTT		0.7954	
17	TAGTCCTGAGGTGCCCGCGATGGACTTTTTTTTTTTTTT		0.6750	
21	TAGTCCTGAGGTGCCCGCGATGGACTTTTTTTTTTTTTT		0.5403	
28	TAGTCCTGAGGTGCCCGCGATGGACTTTTTTTTTTTTTT	cgagatgtgtgtgtaaacagtgg	0.3852	
			2.3959	
1.0	Class 7	CCCHHCCA A HCHHA CHA CCHCHCTC	0.6770	
16	TGTGGGTGGAATGGGGAAGGGAGTGTTTTTTTTTTTTT		0.6773	
22	TGTGGGTGGAATGGGGAAGGGAGTGTTTTTTTTTTT	GCCTTCGAATCTTACTAGCTCTCTC	0.4930	

M.Sc. Thesis – R. Amini; McMaster University – Biochemistry & Biomedical Sciences

40	TGTGGGTGGAATGGGGAAGGGAGTGTTTTTTTTTT	GCCTTCGAATCTTACTAGCTCTCTC	0.2423			
48	TGTGGGTGGAATGGGGAAGGGAGTGTTTTTTT	GCCTTCGAATCTTACTAGCTCTCTC	0.2200			
			1.6326			
	Class 8	3				
23	ACATCCGAAGTTGTCCCGAGGTTGTTTTTTTTTT	GTATGCTTTAAGGGGGTTGTGTC	0.4915			
42	ACATCCGAAGTTGTCCCGAGGTTGTTTTTTTT	GTATGCTTTAAGGGGGTTGTGTC	0.2330			
44	ACATCCGAAGTTGTCCCGAGGTTGTTTTTTTTTTT	GTATGCTTTAAGGGGGTTGTGTC	0.2264			
			0.9509			
	Class					
24	ACAGGCGGAGGTGTTCGCGACCCTGTTTTTTTTTT	GGGGCTTCTAAGGGGGTTGTGTCTG	0.4718			
29	ACAGGCGGAGGTGTTCGCGACCCTGTTTTTTTTTTT	GGGGCTTCTAAGGGGGTTGTGTCTG	0.3741			
46	ACAGGCGGAGGTGTTCGCGACCCTGTTTTTTTT	GGGGCTTCTAAGGGGGTTGTGTCTG	0.2237			
			1.0696			
	Class 1	0				
25	CCAGCATCTTATTAGCTCTCGCTGGTTTTTTTTTTT	CGGGTAAGGGGGTTGTGTCTGCCC	0.4152			
30	CCAGCATCTTATTAGCTCTCGCTGGTTTTTTTTTT	CGGGTAAGGGGGTTGTGTCTGCCC	0.3675			
36	CCAGCATCTTATTAGCTCTCGCTGGTTTTTTTTTTT	CGGGTAAGGGGGTTGTGTCTGCCC	0.2899			
	Class 1	1				
35	AGTGCGTAGCTAAGATGTCTAGCACTTTTTTTTTT	GGCTTCCTAAGGGGGTTGTGTCTGG	0.3021			
39	AGTGCGTAGCTAAGATGTCTAGCACTTTTTTTTTTT	GGCTTCCTAAGGGGGTTGTGTCTGG	0.2481			
			0.5502			
	Class 1	2				
38	ATGTGGGTGGAATGGGGAAGTGGAGTTTTTTTTTTTTT	CGGAGATGTGTGTGAAACAGTGG	0.2492			
47	ATGTGGGTGGAATGGGGAAGTGGAGTTTTTTTTTTTTT	CGGAGATGTGTGTGAAACAGTGG	0.2211			
			0.4703			
	Class 1	3				
43	TAGTCCTGAGGTGCCCGCGATGGACTTTTTTTTT	GGCTTCCTAAGGGGGTTGTGTCTGG	0.2283			
49	TAGTCCTGAGGTGCCCGCGATGGACTTTTTTTTTT	GGCTTCCTAAGGGGGTTGTGTCTGG	0.2048			
			0.4331			
	Class 1	4				
45	AGTGCGTAGCTAAGATGTCTAGCACTTTTTTTTTTT	ATGCTGGGGTATATACAGTCTAGAG	0.2243			
			0.2243			

Table S5. Sequence classes of left domain observed in Top 50 sequences.

Class Name	Sequence	Observed in Class:
LD1	CACGATCCATGTTGTTTACTGGTAG	1
LD2	TGTGGGTGGAATGGGGAAGGGAGTG	2, 3, 4, 5, 7
LD3	TAGTCCTGAGGTGCCCGCGATGGAC	6, 13
LD4	ACATCCGAAGTTGTCCCGAGGTTGT	8
LD5	ACAGGCGGAGGTGTTCGCGACCCTG	9
LD6	CCAGCATCTTATTAGCTCTCGCTGG	10
LD7	AGTGCGTAGCTAAGATGTCTAGCAC	11, 14
LD8	ATGTGGGTGGAATGGGGAAGTGGAG	12

Table S6. Sequence classes of right domain observed in Top 50 sequences.

Class Name	Sequence	Observed in Class:	
RD1	GGAGTGAGCTGGGGGGGGTAGTGTT	1	
RD2	GTAATGCTTCATCTTATTAGCTCTC	2	
RD3	GGGCTCCTTTTAAGTGCGTCGCG	3	
RD4	GTGAGATGTGTGGTGTGGAATGGG	4	
RD5	CGGAGATGTGTGTGAAACAGTGG	5, 6, 12	
RD6	GCCTTCGAATCTTACTAGCTCTCTC	7	
RD7	GTATGCTTTAAGGGGGTTGTGTC	8	
RD8	GGGGCTTCTAAGGGGGTTGTGTCTG	g 9	
RD9	CGGGTAAGGGGGTTGTCTGCCC	10	
RD10	RD10 GGCTTCCTAAGGGGGTTGTCTGG 11, 13		
RD11	ATGCTGGGGTATATACAGTCTAGAG	14	

Table S7. K_d values of reported aptamers for the SARS-CoV-2 spike protein.

No	Identifier	Aptamer	K _d (nM)	Ref
1	This work	DRDA-8/10	0.15	-
2	Yang-2021	nCoV-S1-Apt1	0.33	[73]
3	Minagawa-2022	RBD-Ugu1	1.2	[76]
4	Ferreira-Bravo-2021	FANA-R8–9	1.4	[77]
5	Yang-2022	SCORe	1.73	[78]
6	Chen-2022	RBD/S-A1	1.74	[79]

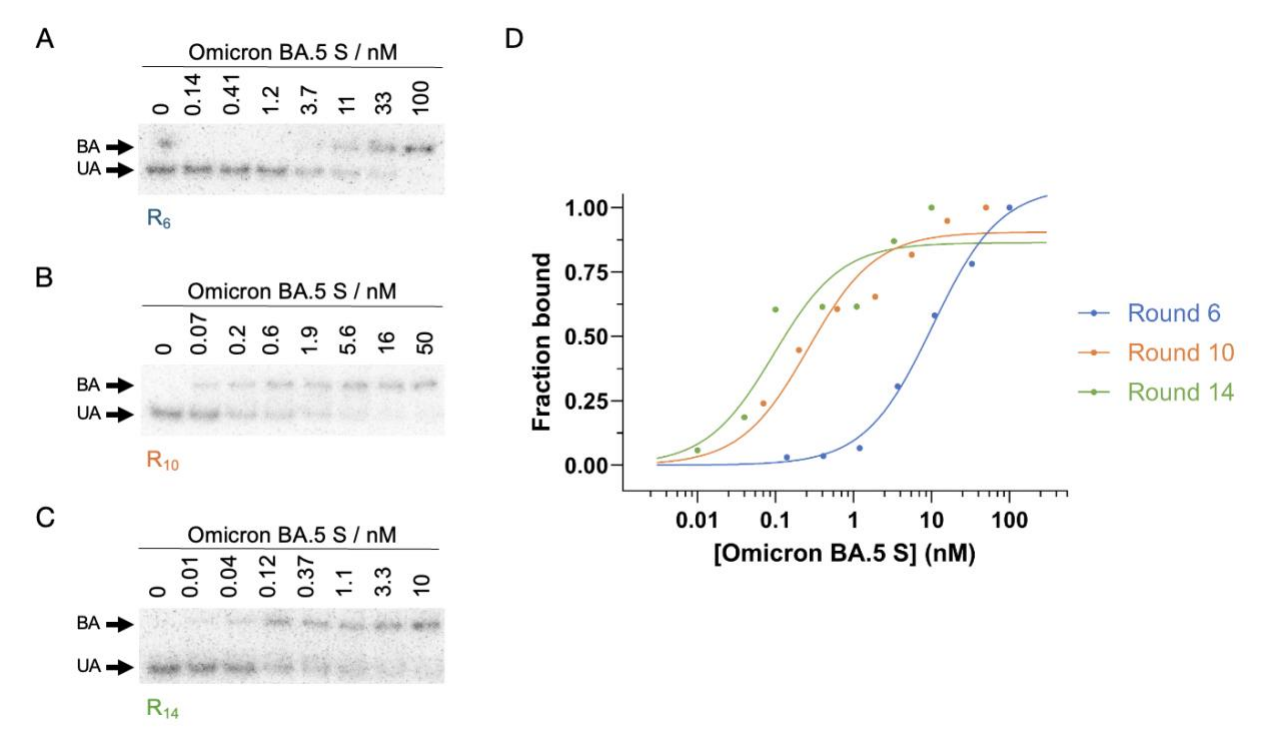


Figure S1. Assessment of binding of selected enriched pools for Omicron BA.5 S protein target. Representative EMSA results showing (A) round 6, (B) round 10, and (C) round 14 binding to S protein. An estimated 100 pM of labelled DNA aptamer was incubated with BA.5 S protein of varying concentrations for 1 hour. Following incubation, the aptamer-protein mixtures were subjected through gel electrophoresis and the individual gels were subsequently imaged. (B) Binding curves of round 6, 10, and 14 pools.

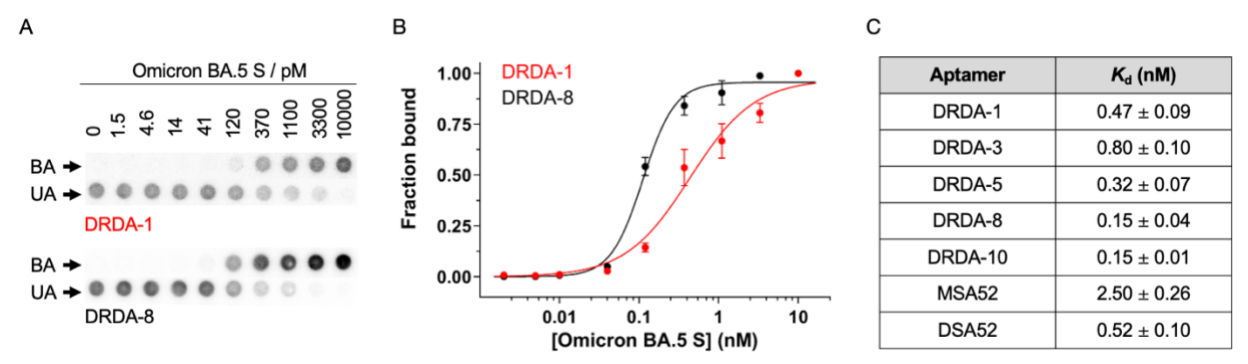


Figure S2. Assessment of binding affinity of top DRD aptamers for the Omicron BA.5 S **protein.** (A) Representative dot blot results of DRDA-1 and DRDA-8 showing binding to S protein. BA: bound aptamer; UA: unbound aptamer. An estimated 100 pM of labelled DNA aptamer was incubated with BA.5 S protein of concentrations ranging from 10-0.0015 nM for 1 hour. Following incubation, the aptamer-protein mixtures were subjected through dot blot filtration and the membranes were subsequently imaged. (B) Binding curves of DRDA-1 and DRDA-8, which were used to determine K_d values for DRD aptamers. (C) K_d values (in nM) of DRDA-1, DRDA-3, DRDA-5, DRDA-8, DRDA-10, MSA52, and DSA52.

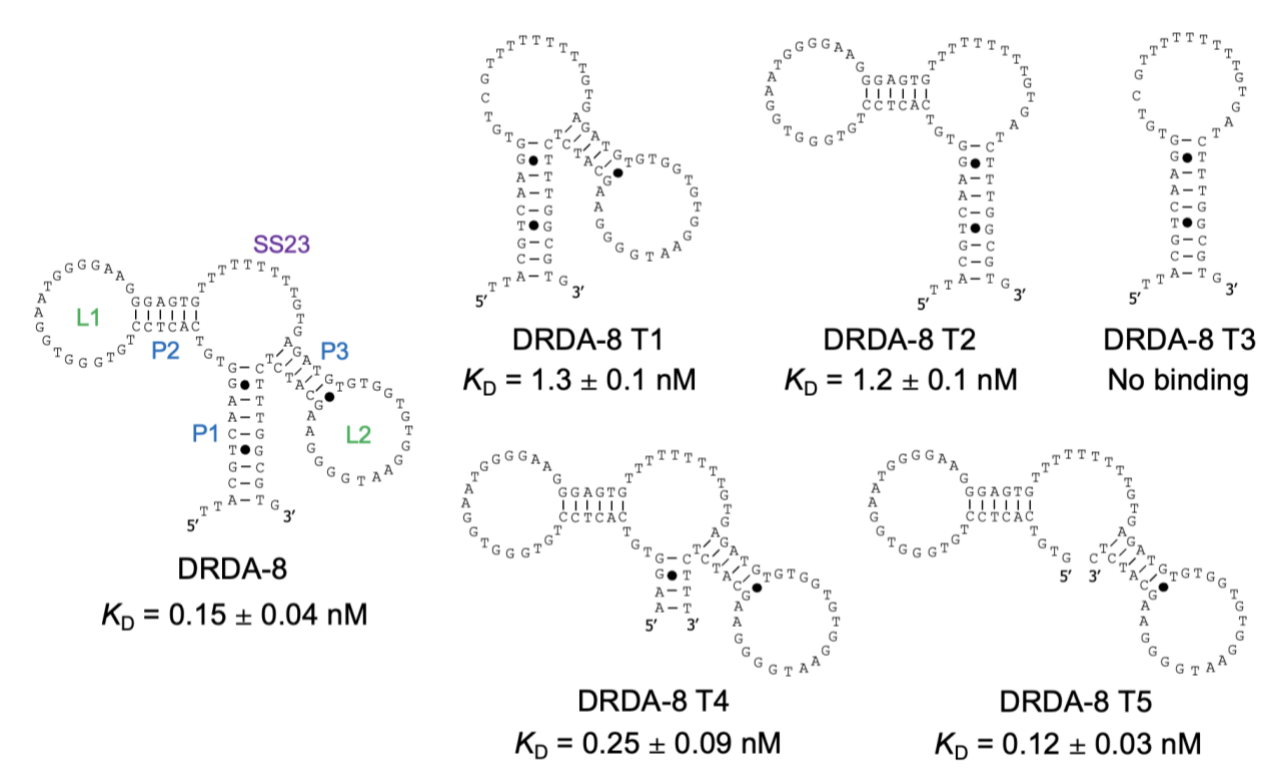


Figure S3. The predicted secondary structure of DRDA-8 and the binding affinity of its truncated mutants. An estimated 100 pM of labelled DNA aptamer was incubated with BA.5 S protein of concentrations ranging from 10-0.0015 nM for 1 hour. Following incubation, the aptamer-protein mixtures were subjected through dot blot filtration and the membranes were subsequently imaged. Bound fractions were quantified and plotted to obtain K_d values.

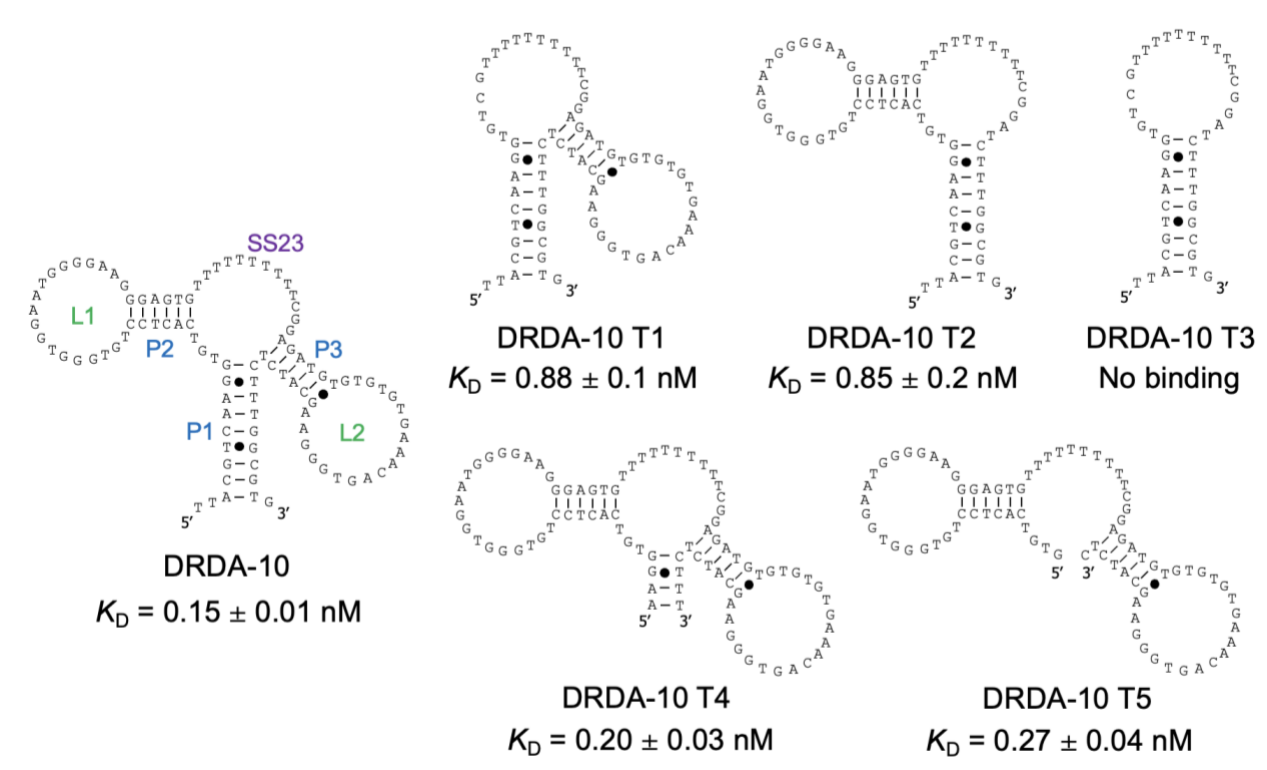


Figure S4. The predicted secondary structure of DRDA-10 and the binding affinity of its truncated mutants. An estimated 100 pM of labelled DNA aptamer was incubated with BA.5 S protein of concentrations ranging from 10-0.0015 nM for 1 hour. Following incubation, the aptamer-protein mixtures were subjected through dot blot filtration and the membranes were subsequently imaged. Bound fractions were quantified and plotted to obtain K_d values.

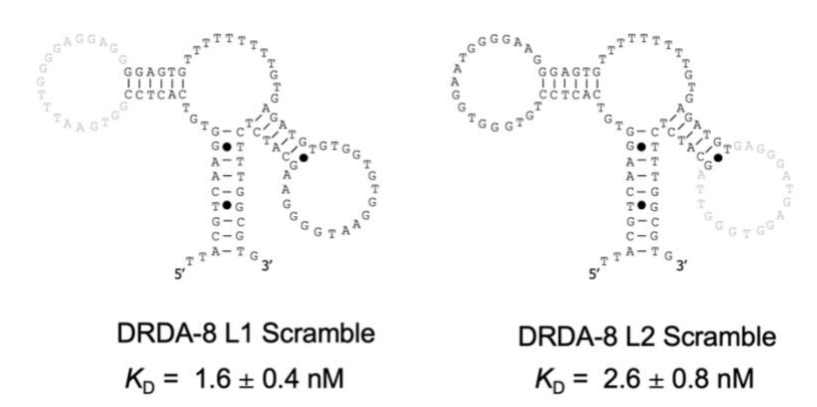


Figure S5. Binding affinity of DRD aptamer mutants with loop scrambled sequences. Scrambled nucleotides are indicated in gray. An estimated 100 pM of labelled DNA aptamer was incubated with BA.5 S protein of concentrations ranging from 10-0.0015 nM for 1 hour. Following incubation, the aptamer-protein mixtures were subjected through dot blot filtration and the membranes were subsequently imaged. Bound fractions were quantified and plotted to obtain K_d values.

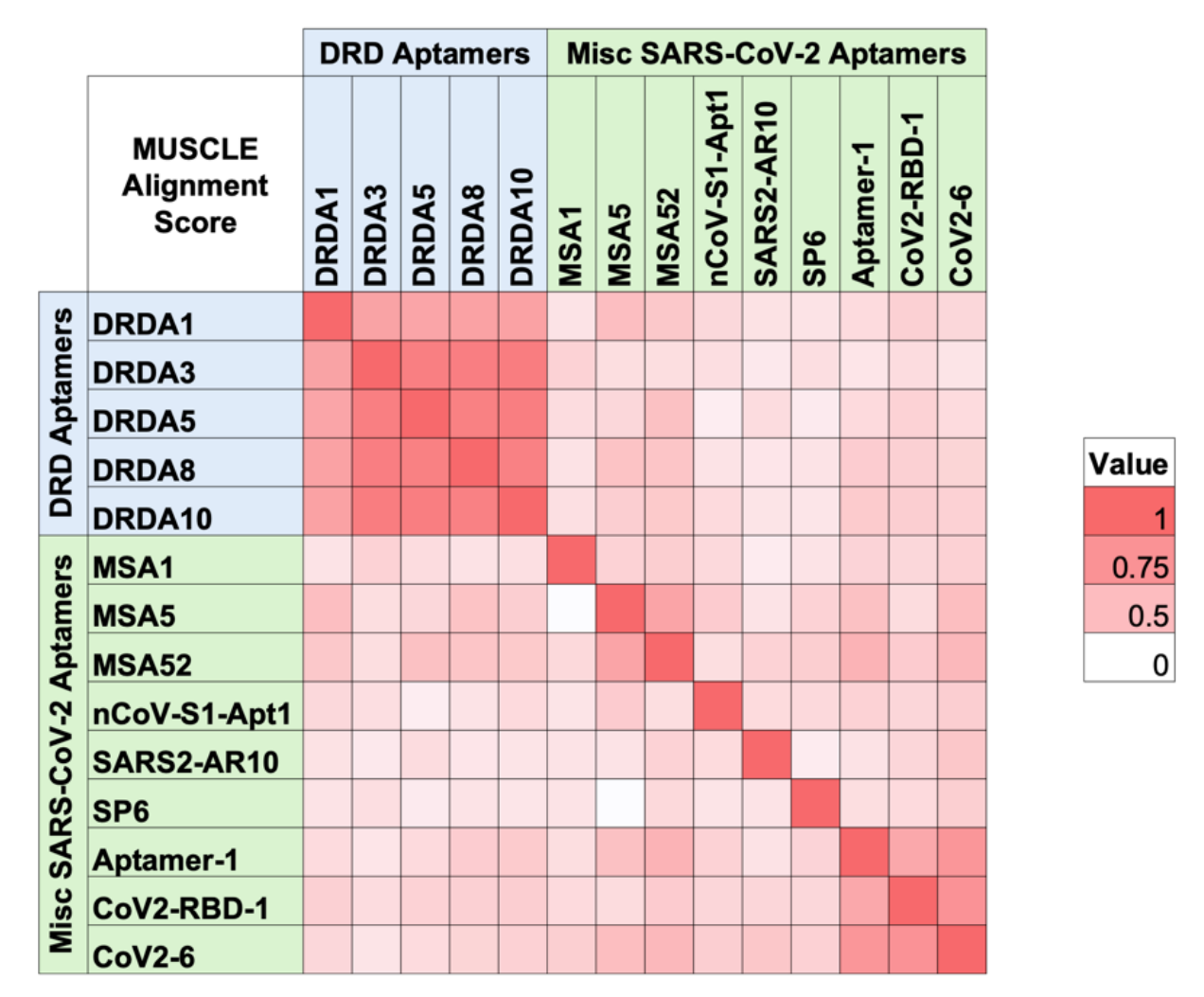


Figure S6. MUSCLE alignment comparison of DRD aptamers to a selection of published SARS-CoV-2 spike aptamer sequences. Heatmap for all sequence pairs where a hit was reported. Sequences of high similarity generate high scores indicated by dark red shading. High alignment scores along the diagonal represents self-alignment.

REFERENCES

- [1] T. Chang, S. He, R. Amini, Y. Li, *Chembiochem* **2021**, 22, 2368–2383.
- [2] T. R. Cech, A. J. Zaug, P. J. Grabowski, *Cell* **1981**, 27, 487–496.
- [3] K. Kruger, P. J. Grabowski, A. J. Zaug, J. Sands, D. E. Gottschling, T. R. Cech, *Cell* **1982**, *31*, 147–157.
- [4] T. R. Cech, Science **1987**, 236, 1532–1539.
- [5] S. Altman, Adv Enzymol Relat Areas Mol Biol 1989, 62, 1–36.
- [6] H. W. Pley, K. M. Flaherty, D. B. McKay, *Nature* **1994**, *372*, 68–74.
- [7] C. Tuerk, L. Gold, Science **1990**, 249, 505–510.
- [8] A. D. Ellington, J. W. Szostak, *Nature* **1990**, *346*, 818–822.
- [9] M. R. Dunn, R. M. Jimenez, J. C. Chaput, *Nature Reviews Chemistry* **2017**, *1*, 76–76.
- [10] E. M. McConnell, I. Cozma, D. Morrison, Y. Li, Analytical Chemistry 2020, 92, 327–344.
- [11] H. Sun, Y. Zu, Molecules 2015, 20, 11959–11980.
- [12] A. D. Gelinas, D. R. Davies, N. Janjic, Current Opinion in Structural Biology 2016, 36, 122–132.
- [13] J. F. Lee, Nucleic Acids Research 2004, 32, 95D 100.
- [14] J. Byun, Life **2021**, 11, 193.
- [15] D. S. Wilson, J. W. Szostak, Annual review of biochemistry **1999**, 68, 611–647.
- [16] M. H. Ali, M. E. Elsherbiny, M. Emara, *IJMS* **2019**, *20*, 2511.
- [17] K.-M. Song, S. Lee, C. Ban, Sensors (Basel, Switzerland) 2012, 12, 612–631.
- [18] C. R. Ireson, L. R. Kelland, Molecular Cancer Therapeutics 2006, 5, 2957 LP 2962.
- [19] V. Thiviyanathan, D. G. Gorenstein, *Prot. Clin. Appl.* **2012**, *6*, 563–573.
- [20] S. Ni, H. Yao, L. Wang, J. Lu, F. Jiang, A. Lu, G. Zhang, IJMS 2017, 18, 1683.
- [21] S. Ni, Z. Zhuo, Y. Pan, Y. Yu, F. Li, J. Liu, L. Wang, X. Wu, D. Li, Y. Wan, L. Zhang, Z. Yang, B.-T. Zhang, A. Lu, G. Zhang, *ACS Appl. Mater. Interfaces* **2021**, *13*, 9500–9519.
- [22] T. D. Pollard, Mol Biol Cell 2010, 21, 4061–4067.
- [23] S. Qian, D. Chang, S. He, Y. Li, *Analytica Chimica Acta* **2022**, *1196*, 339511.
- [24] Z. Zhang, J. Li, R. Amini, A. Mansfield, J. Gu, J. Xia, J. D. Brennan, Y. Li, *Analysis & Sensing* **2023**, *3*, e202300001.
- [25] A. Brown, J. Brill, R. Amini, C. Nurmi, Y. Li, *Angewandte Chemie International Edition* **2024**, *63*, e202318665.
- [26] M. Mammen, S.-K. Choi, G. M. Whitesides, *Angewandte Chemie International Edition* **1998**, *37*, 2754–2794.
- [27] W. Bahnan, L. Happonen, H. Khakzad, V. Kumra Ahnlide, T. de Neergaard, S. Wrighton, O. André, E. Bratanis, D. Tang, T. Hellmark, L. Björck, O. Shannon, L. Malmström, J. Malmström, P. Nordenfelt, *EMBO Mol Med* 2022, 15, e16208.
- [28] Y. Li, Q. Fan, B. Zhou, Y. Shen, Y. Zhang, L. Cheng, F. Qi, S. Song, Y. Guo, R. Yan, B. Ju, Z. Zhang, *iScience* **2022**, *25*, 104431.
- [29] G. Vauquelin, S. J. Charlton, Br J Pharmacol 2013, 168, 1771–1785.
- [30] K. M. Ahmad, Y. Xiao, H. T. Soh, Nucleic Acids Research 2012, 40, 11777–11783.
- [31] M. A. Vorobyeva, A. S. Davydova, P. E. Vorobjev, D. V. Pyshnyi, A. G. Venyaminova, *Int J Mol Sci* **2018**, *19*, 470.
- [32] H. Hasegawa, N. Savory, K. Abe, K. Ikebukuro, *Molecules* **2016**, *21*, 421.
- [33] S. Manochehry, E. M. McConnell, Y. Li, Sci Rep 2019, 9, 17824.

- [34] J. Li, Z. Zhang, J. Gu, H. D. Stacey, J. C. Ang, A. Capretta, C. D. M. Filipe, K. L. Mossman, C. Balion, B. J. Salena, D. Yamamura, L. Soleymani, M. S. Miller, J. D. Brennan, Y. Li, *Nucleic Acids Research* **2021**, *49*, 7267–7279.
- [35] Z. Zhang, R. Pandey, J. Li, J. Gu, D. White, H. D. Stacey, J. C. Ang, C.-J. Steinberg, A. Capretta, C. D. M. Filipe, K. Mossman, C. Balion, M. S. Miller, B. J. Salena, D. Yamamura, L. Soleymani, J. D. Brennan, Y. Li, *Angewandte Chemie International Edition* **n.d.**, *n/a*, DOI 10.1002/anie.202110819.
- [36] J. Li, Z. Zhang, J. Gu, R. Amini, A. G. Mansfield, J. Xia, D. White, H. D. Stacey, J. C. Ang, G. Panesar, A. Capretta, C. D. M. Filipe, K. Mossman, B. J. Salena, J. B. Gubbay, C. Balion, L. Soleymani, M. S. Miller, D. Yamamura, J. D. Brennan, Y. Li, *J. Am. Chem. Soc.* 2022, 144, 23465–23473.
- [37] Y. Zhou, X. Qi, Y. Liu, F. Zhang, H. Yan, Chembiochem 2019, 20, 2494–2503.
- [38] L. Tang, M. Huang, M. Zhang, Y. Pei, Y. Liu, Y. Wei, C. Yang, T. Xie, D. Zhang, R. Zhou, Y. Song, J. Song, *Small Methods* **2023**, *7*, 2300327.
- [39] R. Sullivan, M. C. Adams, R. R. Naik, V. T. Milam, *Molecules* **2019**, *24*, DOI 10.3390/molecules24081572.
- [40] D. M. Cutler, L. H. Summers, M. Sun, S. Liu, X. Wei, S. Wan, M. Huang, T. Song, Y. Lu, X. Weng, Z. Lin, H. Chen, Y. Song, C. Yang, *Angewandte Chemie International Edition* **2021**, *324*, 1495–1496.
- [41] WHO, "World Health Organization. Coronavirus disease 2019 (COVID-19)," 2020.
- [42] A. D. Kaye, C. N. Okeagu, A. D. Pham, R. A. Silva, J. J. Hurley, B. L. Arron, N. Sarfraz, H. N. Lee, G. E. Ghali, J. W. Gamble, H. Liu, R. D. Urman, E. M. Cornett, *Best Practice & Research Clinical Anaesthesiology* 2021, 35, 293–306.
- [43] R. Antia, M. E. Halloran, *Immunity* **2021**, *54*, 2172–2176.
- [44] R. E. Baker, A. S. Mahmud, I. F. Miller, M. Rajeev, F. Rasambainarivo, B. L. Rice, S. Takahashi, A. J. Tatem, C. E. Wagner, L.-F. Wang, A. Wesolowski, C. J. E. Metcalf, *Nat Rev Microbiol* **2022**, *20*, 193–205.
- [45] M. Lotfi, M. R. Hamblin, N. Rezaei, Clinica Chimica Acta 2020, 508, 254–266.
- [46] T. Jefferson, C. B. Del Mar, L. Dooley, E. Ferroni, L. A. Al-Ansary, G. A. Bawazeer, M. L. van Driel, N. S. Nair, M. A. Jones, S. Thorning, J. M. Conly, *Cochrane Database of Systematic Reviews* 2011, DOI 10.1002/14651858.CD006207.pub4.
- [47] C. B. F. Vogels, A. F. Brito, A. L. Wyllie, J. R. Fauver, I. M. Ott, C. C. Kalinich, M. E. Petrone, A. Casanovas-Massana, M. Catherine Muenker, A. J. Moore, J. Klein, P. Lu, A. Lu-Culligan, X. Jiang, D. J. Kim, E. Kudo, T. Mao, M. Moriyama, J. E. Oh, A. Park, J. Silva, E. Song, T. Takahashi, M. Taura, M. Tokuyama, A. Venkataraman, O.-E. Weizman, P. Wong, Y. Yang, N. R. Cheemarla, E. B. White, S. Lapidus, R. Earnest, B. Geng, P. Vijayakumar, C. Odio, J. Fournier, S. Bermejo, S. Farhadian, C. S. Dela Cruz, A. Iwasaki, A. I. Ko, M. L. Landry, E. F. Foxman, N. D. Grubaugh, *Nature Microbiology* 2020, 5, 1299–1305.
- [48] P. Khan, L. M. Aufdembrink, A. E. Engelhart, ACS Synthetic Biology 2020, 9, 2861–2880.
- [49] M. J. Mina, K. G. Andersen, Science (New York, N.Y.) 2021, 371, 126–127.
- [50] D. Dutta, S. Naiyer, S. Mansuri, N. Soni, V. Singh, K. H. Bhat, N. Singh, G. Arora, M. S. Mansuri, *Diagnostics* **2022**, *12*, 1503.
- [51] V. Parvu, D. S. Gary, J. Mann, Y.-C. Lin, D. Mills, L. Cooper, J. C. Andrews, Y. C. Manabe, A. Pekosz, C. K. Cooper, *Frontiers in Microbiology* **2021**, *12*, 2611–2611.

- [52] J. Dinnes, J. J. Deeks, A. Adriano, S. Berhane, C. Davenport, S. Dittrich, D. Emperador, Y. Takwoingi, J. Cunningham, S. Beese, J. Dretzke, L. Ferrante Di Ruffano, I. M. Harris, M. J. Price, S. Taylor-Phillips, L. Hooft, M. M. Leeflang, R. Spijker, A. Van den Bruel, *Cochrane Database of Systematic Reviews* 2021, DOI 10.1002/14651858.CD013705.pub2.
- [53] R. M. Cox, J. D. Wolf, C. M. Lieber, J. Sourimant, M. J. Lin, D. Babusis, V. DuPont, J. Chan, K. T. Barrett, D. Lye, R. Kalla, K. Chun, R. L. Mackman, C. Ye, T. Cihlar, L. Martinez-Sobrido, A. L. Greninger, J. P. Bilello, R. K. Plemper, *Nat Commun* 2021, *12*, 6415.
- [54] M. Marzi, M. K. Vakil, M. Bahmanyar, E. Zarenezhad, *Biomed Res Int* **2022**, 2022, 7341493.
- [55] A. C. Walls, Y. J. Park, M. A. Tortorici, A. Wall, A. T. McGuire, D. Veesler, *Cell* 2020, 181, 281–292.
- [56] D. Wrapp, N. Wang, K. S. Corbett, J. A. Goldsmith, C. L. Hsieh, O. Abiona, B. S. Graham, J. S. McLellan, *Science* 2020, 367, 1260–1263.
- [57] P. Bayat, R. Nosrati, M. Alibolandi, H. Rafatpanah, K. Abnous, M. Khedri, M. Ramezani, *Biochimie* **2018**, *154*, 132–155.
- [58] M. Yüce, N. Ullah, H. Budak, Analyst 2015, 140, 5379–5399.
- [59] A. Ozer, B. S. White, J. T. Lis, D. Shalloway, *Nucleic Acids Research* **2013**, *41*, 7167–7175.
- [60] I. Manea, M. Casian, O. Hosu-Stancioiu, N. de-los-Santos-Álvarez, M. J. Lobo-Castañón, C. Cristea, *Analytica Chimica Acta* **2024**, *1297*, 342325.
- [61] Z. Zhang, J. Li, J. Gu, R. Amini, H. D. Stacey, J. C. Ang, D. White, C. D. M. Filipe, K. Mossman, M. S. Miller, B. J. Salena, D. Yamamura, P. Sen, L. Soleymani, J. D. Brennan, Y. Li, *Chemistry A European J* **2022**, 28, DOI 10.1002/chem.202200078.
- [62] R. Gysbers, K. Tram, J. Gu, Y. Li, Sci Rep 2015, 5, 11405.
- [63] D. E. Huizenga, J. W. Szostak, *Biochemistry* **1995**, *34*, 656–665.
- [64] M. N. Stojanovic, P. de Prada, D. W. Landry, *Journal of the American Chemical Society* **2000**, *122*, 11547–11548.
- [65] L. S. Green, D. Jellinek, R. Jenison, A. Ostman, C. H. Heldin, N. Janjic, *Biochemistry* **1996**, *35*, 14413–14424.
- [66] L. M. Hellman, M. G. Fried, *Nat Protoc* **2007**, *2*, 1849–1861.
- [67] J. Zhu, T. Li, J. Hu, E. Wang, Anal Bioanal Chem 2010, 397, 2923–2927.
- [68] M. Liu, J. Wang, Y. Chang, Q. Zhang, D. Chang, C. Y. Hui, J. D. Brennan, Y. Li, *Angew Chem Int Ed Engl* **2020**, *59*, 7706–7710.
- [69] M. Liu, Q. Yin, Y. Chang, Q. Zhang, J. D. Brennan, Y. Li, Angew Chem Int Ed Engl 2019, 58, 8013–8017.
- [70] K. H. D. Crawford, R. Eguia, A. S. Dingens, A. N. Loes, K. D. Malone, C. R. Wolf, H. Y. Chu, M. A. Tortorici, D. Veesler, M. Murphy, D. Pettie, N. P. King, A. B. Balazs, J. D. Bloom, *Viruses* 2020, 12, 513.
- [71] M. Kohlberger, G. Gadermaier, *Biotechnology and Applied Biochemistry* **n.d.**, *n/a*, DOI 10.1002/bab.2244.
- [72] R. Goyal, R. K. Gautam, H. Chopra, A. K. Dubey, R. K. Singla, R. A. Rayan, M. A. Kamal, *EXCLI J* **2022**, *21*, 1245–1272.
- [73] G. Yang, Z. Li, I. Mohammed, L. Zhao, W. Wei, H. Xiao, W. Guo, Y. Zhao, F. Qu, Y. Huang, *Signal Transduction and Targeted Therapy* **2021**, *6*, 227–227.

- [74] R. Amini, Z. Zhang, J. Li, J. Gu, J. D. Brennan, Y. Li, *Analysis & Ensing* **2022**, 2, e202200012.
- [75] M. Zuker, Nucleic Acids Research 2003, 31, 3406–3415.
- [76] H. Minagawa, H. Sawa, T. Fujita, S. Kato, A. Inaguma, M. Hirose, Y. Orba, M. Sasaki, K. Tabata, N. Nomura, M. Shingai, Y. Suzuki, K. Horii, *Biochemical and Biophysical Research Communications* **2022**, *614*, 207–212.
- [77] I. Alves Ferreira-Bravo, J. J. DeStefano, Viruses 2021, 13, 1983.
- [78] L. F. Yang, N. Kacherovsky, J. Liang, S. J. Salipante, S. H. Pun, *Anal Chem* **2022**, *94*, 12683–12690.
- [79] Y. Chen, X. Yang, J. Liu, D. Zhang, J. He, L. Tang, J. Li, Q. Xiang, *Nucleosides Nucleotides Nucleic Acids* **2023**, *42*, 105–118.